T.R.
BOLU ABANT İZZET BAYSAL UNIVERSITY
INSTITUTE OF GRADUATE STUDIES
Department of Chemistry

STUDY OF SYNTHESIS AND OPTICAL PROPERTIES OF TRANSITION METAL SUBSTITUTED LDH NANOPARTICLES

MASTER OF SCIENCE

AKRAM H M ALMUNİRAWİ

ACADEMIC SUPERVISOR
Prof. Dr. AYŞE MORKAN

BOLU, JULY 2024

APPROVAL OF THE THESIS

STUDY OF SYNTHESIS AND OPTICAL PROPERTIES OF TRANSITION METAL SUBSTITUTED LDH NANOPARTICLES submitted by **Akram H M Almunirawi** and defended before the Examining Committee Members listed below in partial fulfillment of the requirements for the degree of **Master of Science** in **Department of Chemistry, Institute of Graduate Studies of Bolu Abant Izzet Baysal University in 29.07.2024** by

Examining Committee Members	**Signature**
Supervisor Prof. Dr. Ayşe MORKAN Bolu Abant Izzet Baysal University	.....
Member Prof. Dr. Fazilet Devrim ÖZDEMİRHAN Bolu Abant Izzet Baysal University	.....
Member Prof. Dr. Mecit AKSU Düzce University	.....

Prof. Dr. İbrahim KÜRTÜL

Director of Institute of Graduate Studies

I dedicate this research to my dear family, who have always been the cornerstone of my life especially my mother

ETHICAL DECLARATION

In this thesis dissertation that was properly prepared according to the Thesis Writing Rules of Bolu Abant Izzet Baysal University of the Institute of Graduates Studies, I hereby declare that;

- All data, information, and documents presented in the thesis were obtained in accordance with the academic and ethical rules,
- All data, documents, assessments, and results were presented in accordance with the scientific ethical and moral rules,
- All works that were benefitted in the thesis were appropriately cited,
- No alteration was made in the data used,
- Study presented in this thesis is original,

Otherwise, I declare that I accept the loss of all my rights in case any contradiction that may arise against me.

The similarity rate obtained by using the Turnitin program, a plagiarism detection software, is within the limits approved by the University Senate.

_____

AKRAM H M ALMUNIRAWI

ABSTRACT

STUDY OF SYNTHESIS AND OPTICAL PROPERTIES OF TRANSITION METAL SUBSTITUTED LDH NANOPARTICLES

MSC THESIS

AKRAM H M ALMUNİRAWİ

BOLU ABANT IZZET BAYSAL UNIVERSITY

INSTITUTE OF GRADUATE STUDIES

DEPARTMENT OF CHEMISTRY

(SUPERVISOR: Prof. Dr. AYŞE MORKAN)

BOLU, JULY 2024

(xiv + 45)

$Mg_{3-x-y}M_xM'_y/Al_1$ is the general formula of double metal-substituted magnesium aluminum layered double hydroxides. In this study, Mg-Al LDH, where magnesium is substituted by two different metal cations, M (Zn) and M' (Ni or Co), in the brucite-like layers of the LDH. MgZnNiAl LDH and MgZnCoAl LDH were successfully synthesized through the sol-gel method under optimized conditions. The corresponding LDH materials were prepared with different stoichiometry by varying the molar ratios of Mg:Ni and Mg:Co whereas zinc and aluminum concentrations were kept constant.

The as-prepared LDH materials were thoroughly investigated by a range of analytical techniques such as FT-IR spectroscopy, X-ray diffraction and also ultraviolet-visible spectroscopy, which provided a wide understanding of the compositional and structural characteristics of the Mg-Al LDH.

The obtained data of UV-Vis spectroscopy and XRD were utilized to calculate lattice parameters (a and c), crystallite sizes (D), microstrain (ε), positions and displacements of atoms (u), volume of the unit cell (v), band gap, and dielectric constant. XRD data revealed similar patterns for the MgZnNiAl LDH and MgZnCoAl LDH, suggesting that they have common structural backbone, moreover, MgZnNiAl LDH samples showed a higher crystallinity. FT-IR spectra showed the distinct bands corresponding to the vibrational modes of the hydroxyl groups (OH^-) and nitrate (NO_3^-) groups within LDH structure. Moreover, it was found that varying concentrations of metal cations significantly affected the composition, structure, optical properties and functional characteristics of LDH materials.

KEYWORDS: Double metal-substituted, Mg/Zn-Al LDH, Layered double hydroxides, Sol-gel method, XRD, FT-IR.

ÖZET

GEÇİŞ METALİ DEĞİŞİMLİ LDH NANOPARTİKÜLLERİNİN SENTEZİ VE OPTİK ÖZELLİKLERİNİN İNCELENMESİ
YÜKSEK LİSANS TEZİ
AKRAM H M ALMUNIRAWI
BOLU ABANT İZZET BAYSAL ÜNİVERSİTESİ
LİSANSÜSTÜ EĞİTİM ENSTİTÜSÜ
KİMYA ANABİLİM DALI
(TEZ DANIŞMANI: Prof. Dr. AYŞE MORKAN)
BOLU, TEMMUZ - 2024
(xiv + 45)

$Mg_{3-x-y}M_xM'_y/Al_1$, çift metal değişimli Mg-Al tabakalı çift hidroksitlerin (TÇH) genel formülüdür. Bu çalışmada, magnezyum, TÇH'nin brusit benzeri katmanlarında iki farklı metal katyonu (M (Zn) ve M' (Ni ve Co) ile ikame edilerek, MgZnNiAl TÇH ve MgZnCoAl TÇH, optimize edilmiş koşullar altında sol-jel yöntemiyle başarıyla sentezlendi. Karşılık gelen TÇH malzemeleri, çinko ve alüminyumun derişimleri sabit tutularak, Mg:Ni ve Mg:Co metallerinin derişimleri değişen molar oranları kullanılarak hazırlandılar.

Sentezlenen TÇH numuneleri, X-ışını kırınımı (XRD), Fourier dönüşümü kızılötesi spektroskopisi (FT-IR) ve ultraviyole görünür (UV-Vis) spektroskopisi dahil olmak üzere bir dizi analitik teknik kullanılarak kapsamlı bir şekilde karakterize edildi; bu, TÇH'lerin yapısal ve bileşimsel özelliklerinin geniş bir şekilde anlaşılmasını sağladı.

UV-VIS spektroskopi ve XRD verileri, malzemelerin, kristalit boyutlarını (D), kafes parametrelerini (a ve c), mikro gerilimi (ε), atomların konumlarını ve yer değiştirmelerini (u), birim hücrenin hacmini (v), bant aralığı ve dielektrik sabitini hesaplamak için kullanıldı. XRD verileri incelendiğinde, MgZnNiAl TÇH ve MgZnCoAl TÇH için benzer desenlerin elde edildiği ve böylece bu malzemelerin, ortak yapısal omurgaya sahip oldukları, ayrıca MgZnNiAl LDH örneklerinin daha yüksek bir kristallik gösterdiği ortaya konuldu.

FT-IR spektrumları, TÇH yapısındaki hidroksil grupları (OH^-) ve nitrat (NO_3^-) gruplarının titreşim modlarına karşılık gelen farklı tepe noktaları olduğunu gösterdi. Ayrıca bu çalışmada, metal katyonlarının değişen konsantrasyonlarının, TÇH malzemelerinin bileşimini, yapısını, optik özelliklerini ve fonksiyonel karakteristiklerini önemli ölçüde etkilediği bulunmuştur.

ANAHTAR KELİMELER: Çift metal değişimi, Mg/Zn-Al TÇH, Tabakalı çift hidroksitler, Sol-jel yöntemi, XRD, FT-IR.

TABLE OF CONTENTS

Page

APPROVAL OF THE THESIS iii

ETHICAL DECLARATION v

ABSTRACT vi

ÖZET vii

TABLE OF CONTENTS viii

LIST OF FIGURES ix

LIST OF TABLES xi

LIST OF PICTURES xii

LIST OF ABBREVIATIONS AND SYMBOLS xiii

ACKNOWLEDGEMENTS xiiii

1. INTRODUCTION 1

1.1 Layered Double Hydroxide 1
1.1.1 Applications 3
1.1.2 Synthesis 4
1.2 Sol Gel method 7
1.3 Disadvantages of Sol-Gel 8
1.4 Magnesium Aluminum layered double hydroxides 8

2. AIM AND SCOPE OF THE STUDY 10

3. MATERIALS AND METHODS 11

3.1 Chemicals 11
3.2 The Process of Synthesis $Mg_{3-X-Y}m_{\times}M'_{y}/Al_{1}$ LDH via Sol-Gel 11
3.3 Instrumented characterization methods of $Mg_{3-x-y}Zn_{\times}M_{y}/Al_{1}$ LDH 13

4. RESULTS AND DISCUSSION 16

4.1. The efficacy of the sol-gel technique for synthesizing $Mg_{3-x-y}Zn_{\times}M_{y}/Al_{1}$ LDH and the impact of concentration variations 16
4.2. X-Ray Diffraction (XRD) Analysis 20
4.3. Fourier-Transform Infrared Spectroscopy (FT-IR) Analysis 23
4.4. UV-VIS absorbance spectroscopy and Diffuse Reflectance Spectroscopy (DRS) analysis 27
4.5. Structural and optical properties 33

5. CONCLUSIONS 39

6. REFERENCES 41

LIST OF FIGURES

Page

Figure 1.1. Representative structure of an LDH. 1
Figure 1.2. Structure of layered hydroxides. 2
Figure 1.3. Different applications of LDH. 3
Figure 1.4. "Photocatalytic CO_2 Conversion with LDHs: Advances in Synthesis and Efficiency". 4
Figure 1.5. Diagrammatic depiction of the ion exchange/capture mechanism and LDH structure. 6
Figure 1.6. Synthesis of LDH single layers by top-down and bottom-up approaches. 6
Figure 1.7. Procedures for preparing sol-gel. 8
Figure 1.8. Steps of synthesis Mg-Al LDH by electrocoagulation. 9
Figure 3.1. Proceeding of sol-gel to obtain the xerogel. 13
Figure 4.1. Wet gel of Mg_{3-x-y} $Zn_{\times}Ni_y/Al_1$ after hydrolysis and condensation. 17
Figure 4.2. Dried gel of A) $Mg_{2.89}$ $Zn_{0.1}$ $Ni_{0.01}$ Al_1**,** B) $Mg_{2.87}$ $Zn_{0.1}$ $Ni_{0.03}$ Al_1,C) $Mg_{2.85}$ $Zn_{0.1}$ $Ni_{0.05}$ Al_1 obtained after being heated at 150ºC for 24 hours. 17
Figure 4.3. Mixed metal oxides (MMO) of A) $Mg_{2.89}$ $Zn_{0.1}$ $Ni_{0.01}$ Al_1, B) $Mg_{2.87}$ $Zn_{0.1}$ $Ni_{0.03}$ Al_1, C) $Mg_{2.85}$ $Zn_{0.1}$ $Ni_{0.05}$ Al_1 obtained after being heated at 650ºC for 4 hours. 17
Figure 4.4. A) MgZnNi/Al LDH1, B) MgZnNi/Al LDH2, C) MgZnNi/Al LDH3. 18
Figure 4.5. MgZnNi/Al LDH powder after grinding. 18
Figure 4.6. Wet gel of A) $Mg_{2.89}$ $Zn_{0.1}$ $Co_{0.01}$ Al_1, B) $Mg_{2.87}$ $Zn_{0.1}$ $Co_{0.03}$ Al_1, ...18
Figure 4.7. Dried gel of A) $Mg_{2.89}$ $Zn_{0.1}$ $Co_{0.01}$ Al_1, B) $Mg_{2.87}$ $Zn_{0.1}$ $Co_{0.03}$ Al_1, ...19
Figure 4.8. Mixed metal oxides of A) $Mg_{2.89}$ $Zn_{0.1}$ $Co_{0.01}$ Al_1, B) $Mg_{2.87}$ $Zn_{0.1}$ $Co_{0.03}$ Al_1, C) $Mg_{2.85}$ $Zn_{0.1}$ $Co_{0.05}$ Al_1. 19
Figure 4.9. A) MgZnCo/Al LDH1, B) MgZnCo/Al LDH2, C) MgZnCo/Al LDH3. 19
Figure 4.10. XRD pattern of MgZnCo/Al xerogel 20
Figure 4.12. XRD Patterns of MgZnNi/Al LDH. 22
Figure 4.13. XRD Patterns of MgZnCo/Al LDH. 22
Figure 4.14. IR spectra of MgZnNi/Al xerogel. 23
Figure 4.15. IR spectra of MgZnCo/Al xerogel. 24
Figure 4.16. IR spectra of MgZnNi/Al Mixed Metal Oxides (MMO). 24
Figure 4.17. IR spectra of MgZnCo/Al Mixed Metal Oxides (MMO). 25
Figure 4.18. IR spectra of MgZnNi/Al LDH. 26
Figure 4.19. IR spectra of MgZnCo/Al LDH. 26
Figure 4.20. Illustration of the different vibrational modes in MgZnM/Al-NO_3 LDH. 27
Figure 4.21. UV-Vis absorbance spectra of MgZnNi/Al Xerogel. 28
Figure 4.22. UV-Vis reflectance spectra of MgZnNi/Al xerogel. 28
Figure 4.23. UV-Vis absorbance spectra of MgZnNi/Al MMO. 29
Figure 4.24. UV-Vis absorbance spectra of MgZnNi/Al MMO. 29
Figure 4.25. UV-Vis absorbance spectra of MgZnNi/Al LDH. 30
Figure 4.26. UV-Vis reflectance spectra of MgZnNi/Al LDH. 31

Figure 4.27. UV-Vis absorbance spectra of MgZnCo/Al LDH. 32
Figure 4.28. UV-Vis reflectance spectra of MgZnCo/Al LDH.....32
Figure 4.29. Tauc plot for MgZnNi/Al LDH band gap energy. 36
Figure 4.30. Tauc plot for MgZnCo/Al LDH band gap energy. 37

LIST OF TABLES

Page

Table 3.1. $Mg_{3-x-y}Zn_xNi_y/Al_1$ LDH samples. 11
Table 3.2. $Mg_{3-x-y}Zn_xCo_y/Al_1$ LDH samples. 12
Table 4.1. Values of lattice parameters (a and c), crystallite sizes (D) and microstrain (ε). 33
Table 4.2. Values of volume of the unit cell (v), positions and displacements of atoms (u), band gap and dielectric constant (*κ)*. 33
Table 4.3. Values of the atomic packing factor (c/a). 35

LIST OF PICTURES

Page

Picture 3.1. X-Ray Diffractometer: Rigaku Multiflex. 14
Picture 3.2. FT-IR Spectrophotometer: Perkin Elmer and SETARAM (SENSY-Sevo) apparatus. 14
Picture 3.3. UV-Vis Spectrophotometer: Perkin Elmer Lambda 35. 15

LIST OF ABBREVIATIONS AND SYMBOLS

LDHs	**:** Layered Double Hydroxides
$Mg_{3-x-y}M_xM'_y/Al_1$ LDH	**:** Double metal substituted of magnesium aluminium Layered Double Hydroxides
MgZnNi/Al LDH	**:** Magnesium Zinc Nickel Aluminium Layered Double Hydroxides
MgZnCo/Al LDH	**:** Magnesium Zinc Cobalt Aluminium Layered Double Hydroxides
TÇH	**:** Tabakalı Çift Hidroksit
MMO	**:** Mixed Metal Oxides
OER	**:** Oxygen Evolution Reaction
ARRs	**:** Ammonium-Releasing Reagents
TEOS	**:** Tetraethyl Orthosilicate
XRD	**:** X-ray Diffraction
FT-IR	**:** Fourier Transform Infrared Spectroscopy
UV-VIS	**:** Ultraviolet Visible Spectroscopy
ºC	**:** Celsius degree
nm	**:** Nanometer
FWHM	**:** Full Width at Half Maximum
eV	**:** Electron Volt

ACKNOWLEDGEMENTS

I would like to express my sincere gratitude to my research scientific Supervisor, Prof. Dr. Ayşe MORKAN for her invaluable guidance and support throughout this project. Her expertise, insights, and encouragement have been crucial in the successful completion of this work.

I would like to extend my heartfelt thanks to Prof. Dr. Izzet MORKAN for his insightful suggestions and steadfast moral support. I am also grateful to Asst. Prof. Dr. Nevin Soylu KOÇ for her assistance in facilitating the data collection process using the X-ray Diffractometer. Furthermore, I am deeply indebted to Dr. Liska FADLIYANI for her exceptional guidance and support throughout this research. Her invaluable feedbacks were instrumental in the completion of this research.

I would like to convey my sincere appreciation to my family for their encouragement and support throughout my academic journey. In addition, I would like to express my heartfelt gratitude to my esteemed colleagues who were always there to share the joys and challenges with me.

Finally, I express my deepest appreciation to everyone who contributed in any way to the completion of this research. Your contributions are greatly appreciated and have made this achievement possible.

1. INTRODUCTION

1.1 Layered Double Hydroxide

The study on the green chemistry has recently leading to the development of innovative, biocompatible materials and techniques for minimizing or eliminating chemical substances' negative impacts. Because of their unique characteristics, bio safe and environmentally friendly nanomaterials reveal the best applicability [1], Layered double hydroxides, which are also known as LDHs, are fascinating compounds with two-dimensional topologies which have attracted study from a diverse array of chemical fields. In general the formula for an LDH is $[M^{+2}{}_{1-x}\ M^{+3}{}_{x}\ (OH)_2]^{x+}\ (An^-)_{x/n}.mH_2O$, the notation M^{2+} refers to divalent cations (such as: Co^{2+}, Ni^{2+} and Mg^{2+}), M^{3+} refers to trivalent cations (such as: Fe^{3+}, Al^{3+} and Mn^{3+}) while An^- represents the anions located in the interlayer (such as: NO_3^-, CO_3^- and X^-) [2][3] as shown below in Figure (1.1).

The formula for the x value is, (0.2-0.33). This number is attributed to the anion exchange capacity, or charge density, of the hydroxide basal layer. Because M^{+3} has been exchanged for M^{+2}, On their surface, the LDHs layer exhibits positive charge diffusion. Anions and water molecules intercalate to neutralize the interlayer [4].

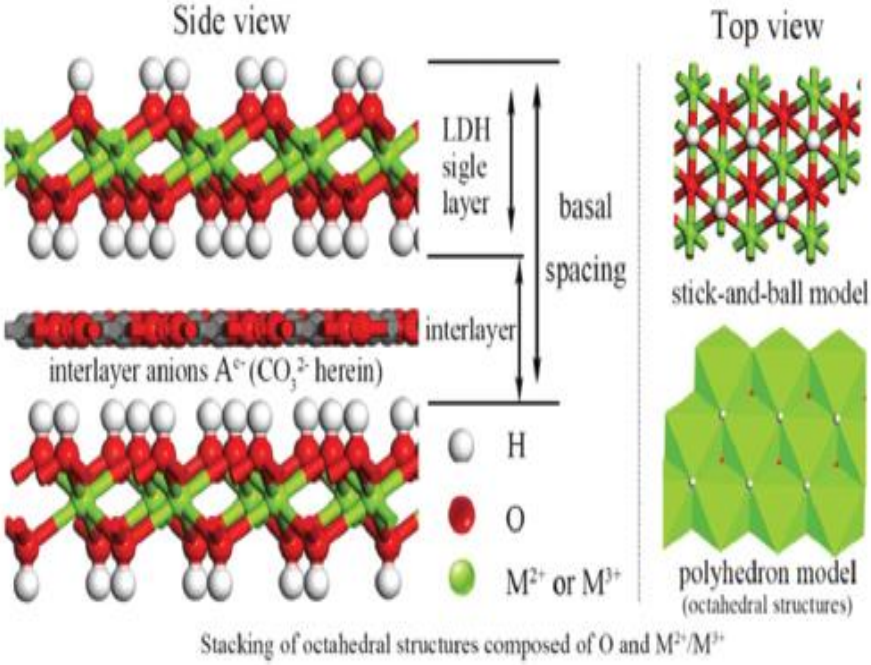

Figure 1.1. Representative structure of an LDH [5].

The layered double hydroxide LDH's abundant hydroxyl groups and interlayer anions can improve surface precipitation when combined with metal ions. The adsorption capacity of LDHs may be restricted by their bulk/granular structure, as they form thick multilayered stacking. By providing a matrix for loading LDH, magnetic biochar can aid in reaching a high level of pollution removal [6].

One advantage of LDHs over other layered materials is their ability to create a variety of compositions and metal-anion combinations. LDHs also possess unique qualities such as excellent chemical stability, pH-sensitive solubility, superior biocompatibility, among others [7].

Synthetic materials called hydrotalcite-like compounds, or LDHs for short, are derived from natural hydrotalcite, or $Mg_2AlOH(CO_3)$. The ability of LDHs to interchange interlayer anions is a unique characteristic that has earned them the moniker anionic clays [8].

Hydrotalcite is an anionic clay with zinc/aluminum hydroxide sheets and hydrated chloride anions. Its positive surface charge allows it to adsorb organic and inorganic anions, useful for removing organic pollutants. Adsorption occurs through electrostatic and hydrophobic interactions. Factors influencing this process include surface structural groups, surfactant molecular structure, and the aqueous phase's content of electrolyte, temperature , and pH [9]. As shown in Figure (1.2).Under low stress circumstances, LDH exhibits outstanding anti-wear properties; but, in high load scenarios, its load-bearing ability decreases [10].

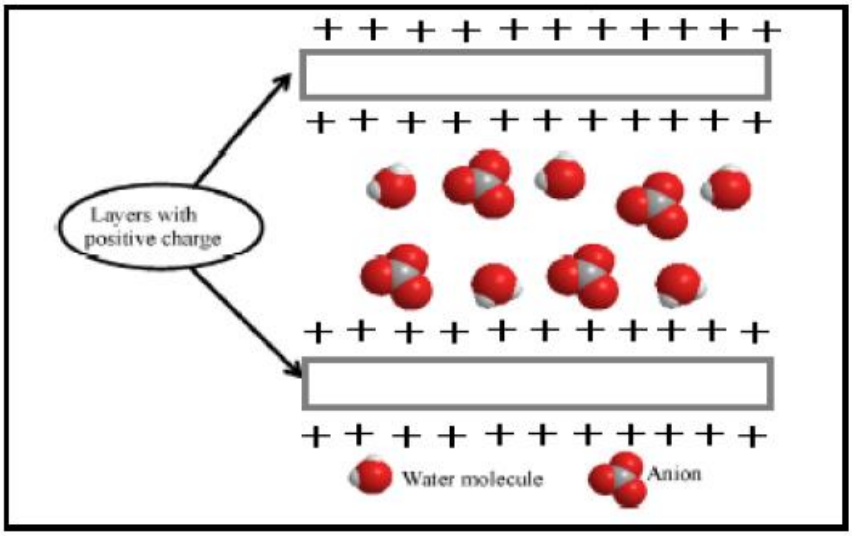

Figure 1.2. Structure of layered hydroxides [9].

1.1.1 Applications

These clays find extensive applications in biotechnology, medicine (particularly in drug delivery and release), environmental remediation, fuel cells, sensors, oxygen evolution reaction (OER), catalyst precursors, and energy storage, among other fields [8]. Moreover, they have been thoroughly investigated in the domains of photochemistry, separation technology, catalysis, polymer additives, anticorrosion coatings, and drug delivery for a variety of pharmaceutically active substances, as well as in cancer treatment [11]. As presented in Figure (1.3).

Figure 1.3. Different applications of LDH [7].

Various organic compounds can be incorporated inside the interlayer parts of the LDH, generating an environment conducive to the integration of metal ions or complexes. This characteristic enables metal species to immobilize on the outer layer of LDH, yielding composite materials with improved functions and characteristics. Thus, employing LDH as metal complexes' support materials widens the scope across various domains, including sensors, energy storage, encompassing electrocatalysis, and environmental applications. Furthermore, LDH's layered structure offers a unique platform for deliberately introducing various anions, enhancing its versatility and functionality, capable of altering LDH's characteristics and functionalities [12].

Stratified layered double hydroxides (LDHs) materials have been regarded as promising applicants for NTP-catalysis, particularly in processes such as ammonia synthesis and CO_2 conversions, as illustrated in Figures (1.4). This is attributed to their abundant hydroxyl groups and adjustable surface electronic structure, coordinated unsaturated active sites (which might help with metal dispersion), and basicity [13][14].

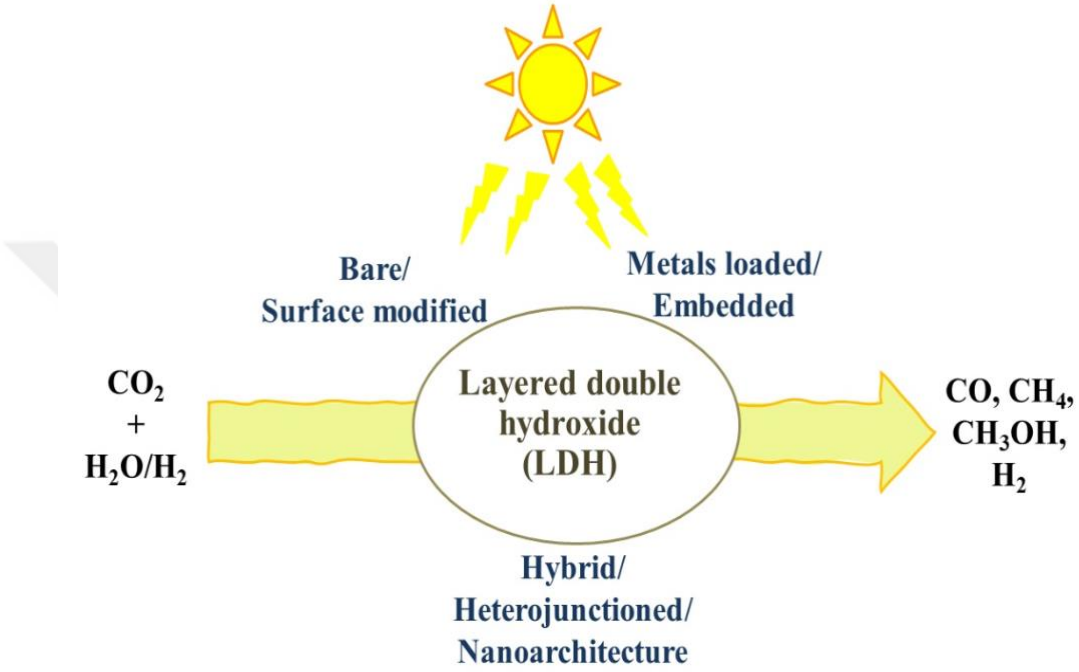

Figure 1.4. "Photocatalytic CO_2 Conversion with LDHs: Advances in Synthesis and Efficiency" [15].

LDHs have gained significant attention for removing environmental contaminants, particularly phosphate ions, due to increasing pollution concerns. Researchers have studied phosphate ion removal using various sorbents, such as activated carbon, silicates, iron oxides, and dried plant particles [16].

Compared to other layered materials, layered double hydroxides are thought to be special because different It is possible to construct hybrid materials, which have unique properties like catalytic activity, shape-selective ion exchange, high surface area, and memory effect [7].

1.1.2 Synthesis

While there are many methods for producing LDHs, urea hydrolysis, ion exchange, hydrothermal and co-precipitation synthesis are the most commonly

used. To fit certain applications, LDHs can be manufactured using a variety of metal combinations, depending on the metals integrated and the methods used for preparation. Additionally, different structural, chemical, and photoelectric characteristics might arise from these combinations. The introduction of a third metal has been discovered to modify the optical characteristics, UV-Vis absorbance spectra and the catalytic characteristics of the LDH in its layered framework [16], as shown in Figure (1.6).

The hydrothermal methods that rely on ammonium-releasing reagents (ARRs)—usually urea or hexamethylene tetramine—are especially fascinating among them due to their ability to generate massive, highly crystalline particles [17]. In many chemical processes, LDHs and the mixed metal oxide that obtained from the thermal decomposition process have been employed as in many fields as essential catalysts, yielding favorable outcomes. Furthermore, LDHs find application in a diverse range of scientific and technological fields, including PVC additives, antacids, flame retardants, and hybrid composites [18].

Co-precipitation is frequently accomplished by gradually adding metal nitrate solutions to a hydroxide and carbonate solution. Due to the slow adding rate, it may take an hour or longer to precipitate the LDH, which results in an uneven aging period for the precipitate. When there isn't an extra aging step, as demonstrated by Valim et al., the crystallite size distribution is wider [19].

The anion exchange method replaces intercalated anions in LDH with target anions by stirring prepared LDH in the desired anion solution, useful when co-precipitation is impractical. The reconstruction method uses LDH's shape memory. Calcining LDH at 400–500°C removes intercalated anions and water, converting hydroxides to oxides. When dissolved in water or target anion solution these oxides are regenerate the LDH structure, effectively intercalating specific target anions [15], as shown in Figure (1.5).

Coprecipitation and hydrothermal synthesis are frequently used in conjunction with urea hydrolysis. Berber et al. discovered that uniform particles were produced by adjusting urea content, age, and M^{2+}:M^{3+} molar ratios. In other investigations, Ni-Al-Mg hydrotalcite was calcined via coprecipitation and urea hydrolysis [21].

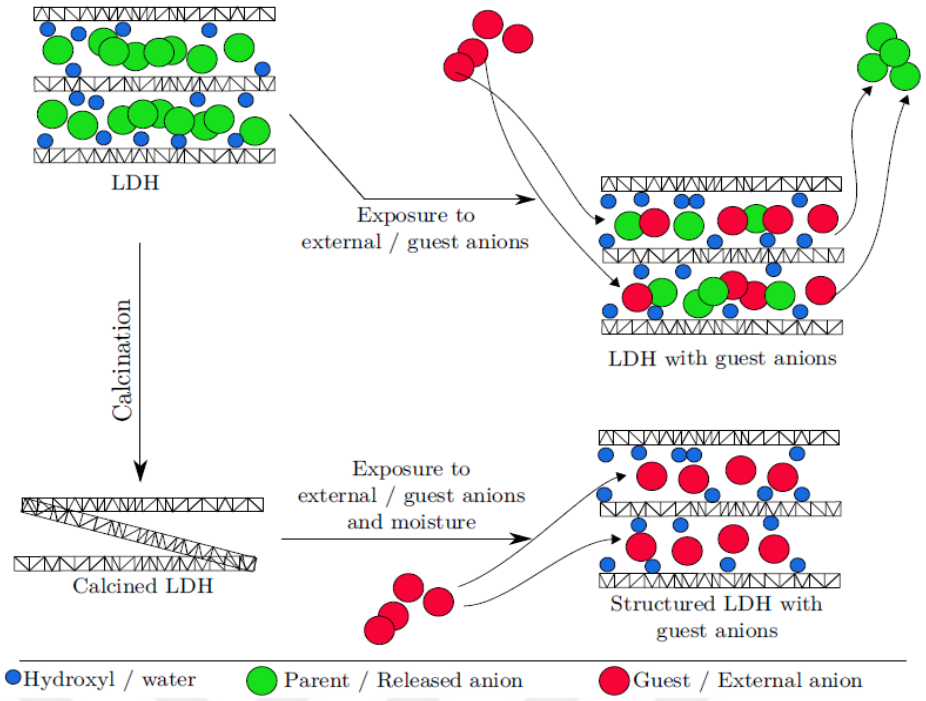

Figure 1.5. Diagrammatic depiction of the ion exchange/capture mechanism and LDH structure [20].

Inayat et al. was examined the Zinc-Aluminum LDHs with nitrate interlayer anion, using urea hydrolysis for precipitation. They showed that synthesis times affect the type of interlayer anion which could be either nitrate or carbonate. However, the steady existence of carbonate from urea limits this method's wide application [22].

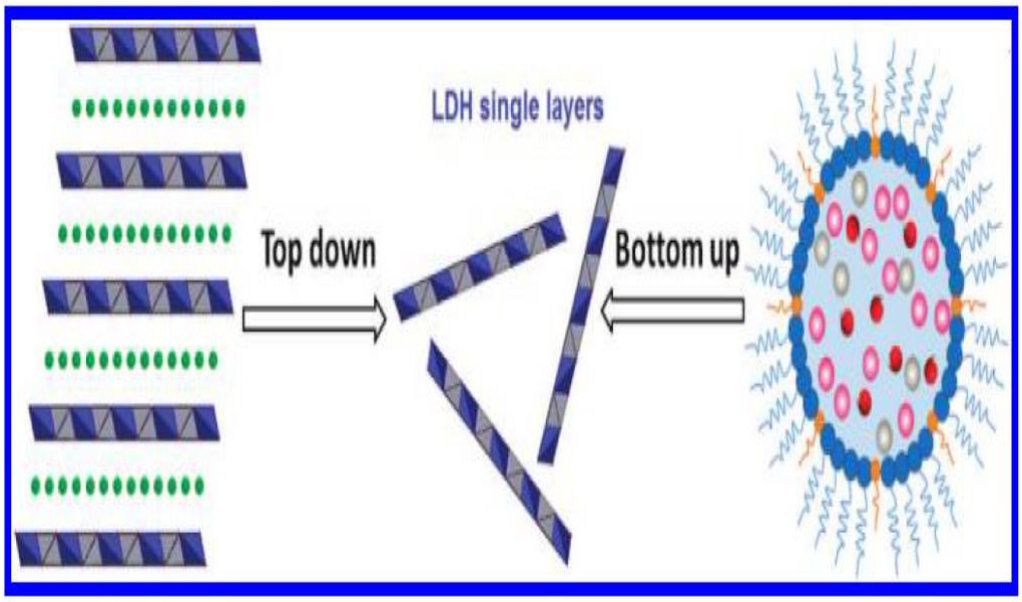

Figure 1.6. Synthesis of LDH single layers by top-down and bottom-up approaches [24].

It is commonly known that the synthesis process has the ability to alter and manipulate the structure, composition, and specific features of LDH. The synthesis process can be primarily divided into two categories: (1) solid-state synthesis technique and (2) liquid phase synthesis technique. The mechanochemical process used in the solid state synthesis approach uses both wet and dry milling techniques [23].

Although using less liquids results in less pollution, this approach is costly and has significant drawbacks, including nonuniform LDH structure and structural deformation. On the other hand, because of its affordability, ease of usage, and capacity to deliver the primary advantages of consistent and comprehensive structural morphology of layered double hydroxide, the synthesis in liquid phase technique is a popular and effective strategy. Depending on the type of reaction, the liquid phase preparation methodology able to be further subdivided into several synthesis techniques [24].

1.2 Sol Gel Method

Sol-gel processing was created by Ebelman and Graham in the middle of 1800s who examined silica gels. Tetraethyl orthosilicate (TEOS), Si $(OC_2H_5)_4$, was degraded to create SiO_2 in an acidic environment. The outcome, as these early researchers observed, was a "glass-like material." [25]. The sol–gel synthesis method for LDHs was developed by Prince et al.; it yields materials with confined pore size distributions ranging from 3 to 4 nm and surface areas up to 290 m^2/g, and particular metallic cations. This results in nano capsule morphology rather of the usual platelet-like particles [26].

A colloidal system is known as sol where the dispersion medium is in liquid phase, and the dispersed phase consists of small molecules or particles that have polymerized within a size ranging from 1 μm to 1 nm. On the other hand, a gel is a network of coherent solid that immobilizes a liquid phase continuously. The subsequent stages in a sol-gel process involve synthesizing the sol by hydrolysis process, transitioning it into the state of sol-gel, drying the gel, and converting it into a calcined substance [27], as shown in Figure (1.7). The method is widely recognized because it can be easily synthesized at low temperatures. Using precipitating agents, sols are transformed into gel in this bottom-up method. The particles shrank in size from Pico to nanometers [1].

The sol-gel process is gaining traction for its advantages: low-temperature processing ensures higher purity and stoichiometry, volatile precursors yield high-purity materials, miscible precursors enable homogeneous doping control, and mild chemical conditions simplify the procedure. It allows for porous material synthesis through organic incorporation and versatile shaping into monoliths, films, and fibers. Additionally, at low temperatures, it makes the production of porous and nanocrystalline materials easier [28].

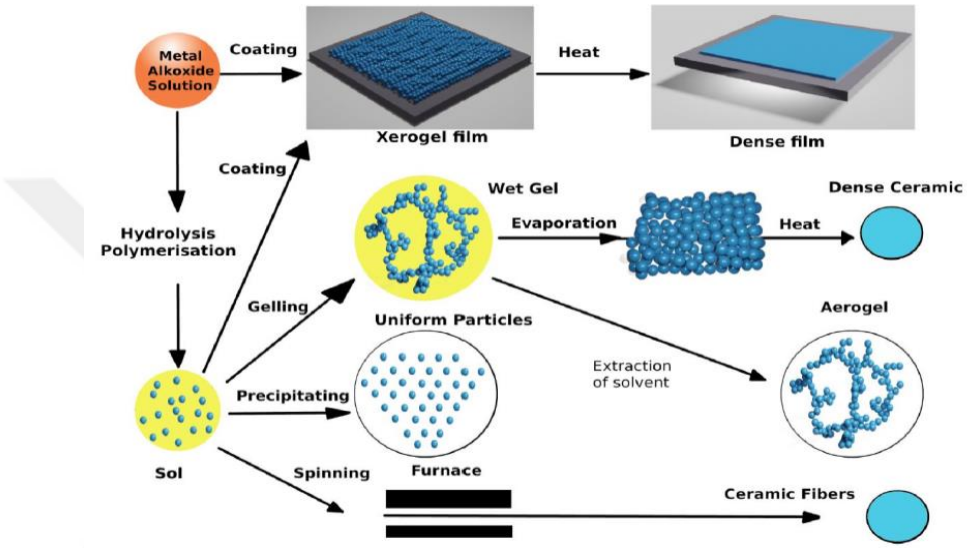

Figure 1.7. Procedures for preparing sol-gel [29].

1.3 Disadvantages of Sol-Gel

Despite its advantages, sol-gel processing has a number of drawbacks, including poor kinetics, limited wear resistance, weak bond formation, and a laborious, drawn-out process that needs extra care during the drying and aging stages. Because of capillary strains, volume loss during densification may result in shrinkage and surface cracking. Large-scale applications are limited by costly and moisture-sensitive precursors, particularly in optical coatings. Furthermore, a number of chemical processes may result in undesirable byproducts, which lower the quality of the material [30].

1.4 Magnesium Aluminum Layered Double Hydroxides

Magnesium/Aluminum LDH was the first layered double hydroxide (LDH) to be found; Hochstetter made this discovery in Sweden. The compound has the formula $Mg_6Al_2(OH)_{16}CO_3$ $4H_2O$. In 1969, Allmann examined the LDH's single-

crystal structure and confirmed its layered structure. Because of the development of synthetic processes, Researchers have explored substituting the original divalent metal, such as Mg^{2+}, with alternative divalent cations like Zn^{2+}, Fe^{2+}, Cu^{2+}, as well as replacing the trivalent metals, exemplified by Al^{3+}, with La^{3+}, Fe^{3+}, and even incorporating tetravalent metals such as Sn^{4+} and Ti^{4+} [31].

Magnesium is the most common M^{2+} metal in hydrotalcites, with aluminum typically occupying the M^{3+} positions. In Mg-Al hydrotalcite, Al partially replaces Mg in the brucite structure, creating a charge imbalance that is countered by various anions namely nitrate, carbonate, sulfate, chloride, and hydroxide, within the interlayer of LDHs, along with water [32].

By altering the metal species and anions, hydrotalcite's characteristics are easily changed. Researchers have modified the characteristics of hydrotalcite for use as catalysts, supports for catalysts, anion exchangers, adsorbents, and plastic additives by substituting metals including Zn, Co, Cu, Ni, Cr, and Fe for Mg and Al. Because of its superior catalytic qualities, Mg-Al hydrotalcite, functions particularly effectively as a heterogeneous catalyst in base-catalyzed processes [22].

Indeed, the electrocoagulation (EC) technique has been found to produce Mg–Al LDH in recent investigations, as shown in Figure (1.8). Electrocoagulation is a branch of electrochemical synthesis processes that offers an economically viable alternative. It relies on the destabilization of suspended. It entails dissolving sacrificial metal anodes with ions in solution to create coagulants in situ [12].

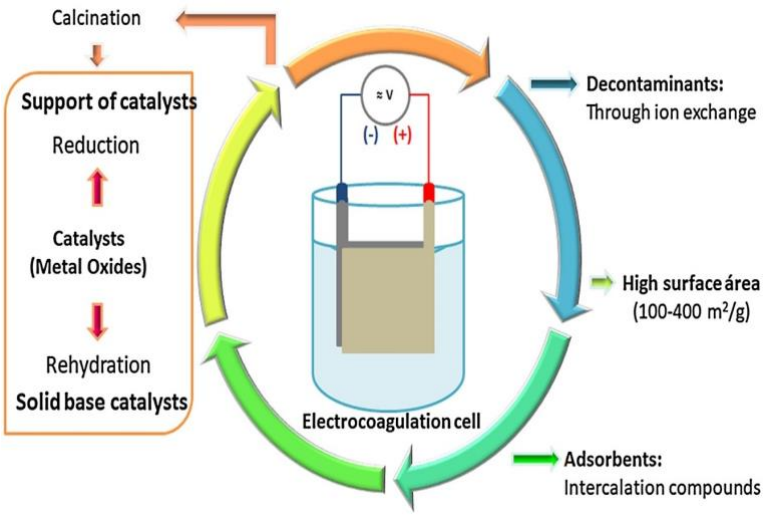

Figure 1.8. Steps of synthesis Mg-Al LDH by electrocoagulation [33].

2. AIM AND SCOPE OF THE STUDY

This study has two primary objectives. Firstly, we aim to successfully synthesize $Mg_{3-x-y}Zn_{\times}Ni_{y}/Al_{1}$ LDH and $Mg_{3-x-y}Zn_{\times}Co_{y}/Al_{1}$ LDH nanoparticles with varying concentrations of Mg, Ni and Co by using the sol-gel method under optimized conditions. Secondly, we intend to thoroughly characterize the synthesized LDH nanoparticles by applying various analytical techniques, such as X-ray Diffraction (XRD), Fourier Transform Infrared (FT-IR) spectroscopy, Ultraviolet-Visible (UV-Vis) spectroscopy and Diffuse Reflectance Spectroscopy (DRS). Thereafter, the obtained data will be utilized to calculate several optical and structural properties, such as crystallite sizes, lattice parameters (a and c), microstrain, positions and displacements of atoms, unit cell volume, optical band gap energy and dielectric constant.

3. MATERIALS AND METHODS

3.1 Chemicals

All the chemicals and materials were procured from Merck GMBH. Magnesium nitrate hexahydrate ($Mg(NO_3)_2 \cdot 6H_2O$), Zinc nitrate hexahydrate ($Zn(NO_3)_2 \cdot 6H_2O$), Nickel nitrate hexahydrate ($Ni(NO_3)_2 \cdot 6H_2O$), Cobalt nitrate hexahydrate ($Co(NO_3)_2 \cdot 6H_2O$), Aluminium nitrate nonahydrate ($Al(NO_3)_3 \cdot 9H_2O$), Citric acid ($C_6H_8O_7H_2O$) and Ethylene glycol ($C_2H_6O_2$). Deionized water was employed in this experiment. The deionized water utilized in the experiment underwent a purification process involving distillation. All the reagents were calculated stoichiometrically and employed without purification.

The magnetically Teflon-coated glasswares were utilized in the experiment. Prior to use, the glassware underwent a thorough cleaning process. This process involved washing the glassware with distilled water, followed by rinsing with ethanol, and then drying the glassware in an oven.

3.2 The Process of Synthesis $Mg_{3-x-y}M_xM'_y/Al_1$ LDH via Sol-Gel

The synthesis process of the double metal substituted compound $Mg_{3-x-y}M_xM'_y/Al_1$ LDH through the sol-gel method involved the preparation of numbers of each MgZnNi/Al LDH and MgZnCo/Al LDH with various stoichiometries. By adjusting the molar ratio of magnesium to nickel and magnesium to cobalt, the amount of magnesium was reduced, while the amounts of the substituting metals nickel and cobalt, were proportionally increased to maintain the total molar count of all metals in the layered double hydroxide compounds at three across all $Mg_{3-x-y}M_xM'_y/Al_1$ LDH different concentrations. As shown in Table 3.1 and 3.2.

Table 3.1. $Mg_{3-x-y}Zn_xNi_y/Al_1$ LDH samples.

LDH Name	Concentration
MgZnNiAl LDH1	$\mathbf{Mg_{2.89}\ Zn_{0.1}\ Ni_{0.01}\ Al_1}$
MgZnNiAl LDH2	$\mathbf{Mg_{2.87}\ Zn_{0.1}\ Ni_{0.03}\ Al_1}$
MgZnNiAl LDH3	$\mathbf{Mg_{2.85}\ Zn_{0.1}\ Ni_{0.05}\ Al_1}$

Table 3.2. $Mg_{3-x-y}Zn_xCo_y/Al_1$ LDH samples.

LDH Name	Concentration
MgZnCoAl LDH1	$\mathbf{Mg_{2.89}\ Zn_{0.1}\ Co_{0.01}\ Al_1}$
MgZnCoAl LDH2	$\mathbf{Mg_{2.87}\ Zn_{0.1}\ Co_{0.03}\ Al_1}$
MgZnCoAl LDH3	$\mathbf{Mg_{2.85}\ Zn_{0.1}\ Co_{0.05}\ Al_1}$

The double metal substituted $Mg_{3-x-y}Zn_xM_y/Al_1$ LDH synthesizing was carried out through sol-gel process. Magnesium nitrate hexahydrate, zinc nitrate hexahydrate, nickel nitrate hexahydrate, cobalt nitrate hexahydrate and aluminium nitrate nonahydrate were allowed to dissolve in 50 mL of dionized water to obtain a precursor solution of metal ions. The precursor solutions were prepared in the desired molar ratios to create the required concentrations for the six LDH samples of $Mg_{3-x-y}\,Zn_xNi_y/Al_1$ LDH and $Mg_{3-x-y}\,Zn_xCo_y/Al_1$ LDH.

The mixed solutions were then subjected to vigorous magnetic stirring for 1 hour at 80°C on a hot plate. During this step, 10 ml of citric acid ($C_6H_8O_7{\cdot}H_2O$, 0.2M) was added sequentially to the mixed solutions. This heating and stirring step, along with the addition of citric acid, was crucial for the formation of a stable, homogeneous sol. After that, 2 mL of complexing agent; ethylene glycol was poured to the homogeneous mixture subsequently and continuously mixed at 150°C until the solution was completely evaporated, and form the gel-like precursor. The formed colored gels were then dried in an oven at 105°C for 24 hours.

The dried gels were then ground up and were underwent heat treatment in a furnace at 650°C for a duration of 4 hours, resulting in the production of the desired mixed metal oxides (MMOs).

The MMO powders were rehydrated using deionized water. The resulting mixture was mixed continuously for 6 hours at 50°C. Finally, the homogeneous solution was introduced to oven and dried for 12 hours at 70°C to successfully acquire the dry LDH powder samples. Controlling the drying process and thermal treatment can produce fine, high-surface-area powder materials.

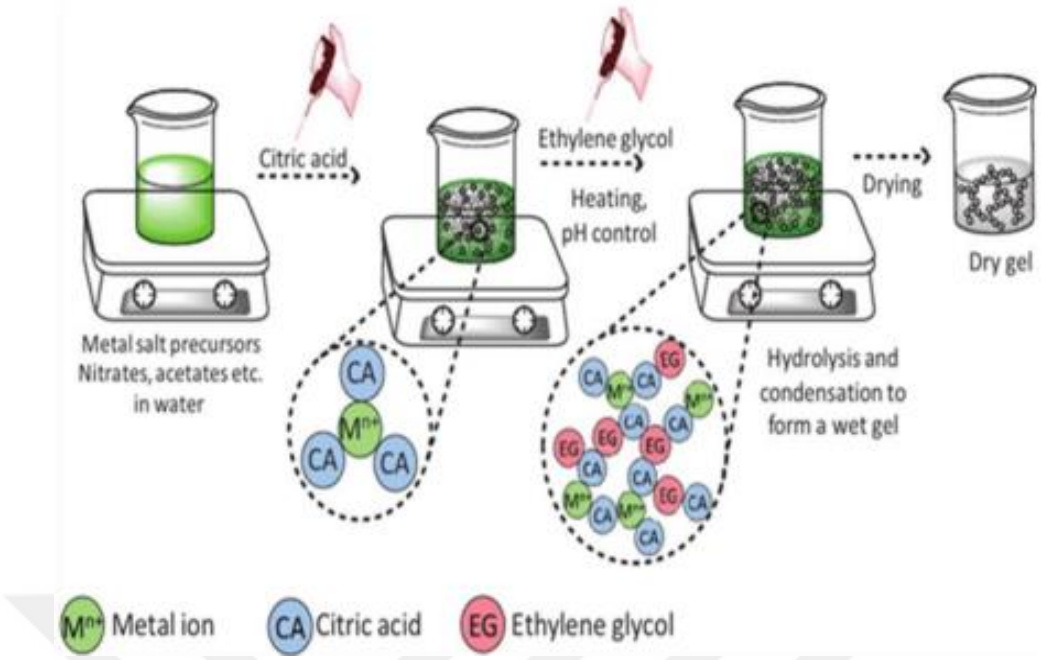

Figure 3.1. Proceeding of sol-gel to obtain the xerogel.

3.3 Instrumental Characterization Methods of $Mg_{3-x-y}Zn_xM_y/Al_1$ LDH

The characterization of $Mg_{3-x-y}Zn_xM_y/Al_1$ LDHs includes the use of several of analytical analysis and techniques, including X-ray diffraction (XRD), Fourier-Transform Infrared spectroscopy (FT-IR), and UV-Vis spectroscopy. These techniques collectively provide a detailed understanding of composition, structure, properties, and behavior of Mg-Al LDHs in different applications.

The XRD analysis reveals the structural properties and also the phase composition of the Mg-Al LDHs [34]. FT-IR spectroscopy is conducted to investigate the functional groups and chemical bonding within the Mg-Al LDH structure [35]. While the UV-Vis analysis has been crucial in evaluating the optical properties of LDH compounds [36].

3.3.1 X-ray diffractometer (XRD)

X-ray powder diffraction analysis was conducted at room temperature to investigate the purity and structural characteristics of synthesized materials. X-ray diffraction patterns were acquired using a Rigaku Multiflex 2 kW diffractometer. The diffractometer was operated at 200 VAC, 1-phase, 30A, 50Hz power supply.

1.5418 Å wavelength for Cu-Kα radiation was used, and the scans were performed over an angular range of 5 to 80.

Picture 3.1. X-Ray Diffractometer: Rigaku Multiflex.

3.3.2 Fourier-transform infrared spectroscopy (FT-IR)

FT-IR spectrophotometer Perkin Elmer was performed to record the infrared spectrum of final products' in the wavenumber ranging between of 4000 to 400 cm^{-1}. To prepare the samples for IR analysis, a pellet was made using a 0.1500: 0.0010 (weight/weight) ratio of potassium bromide (KBr) to the product. The sample pellet was created by pressing the product and oven-dried, spectroscopic grade KBr.

Picture 3.2. FT-IR Spectrophotometer: Perkin Elmer and SETARAM (SENSY-Sevo) apparatus.

3.3.3 Ultraviolet-Visible Spectroscopy

UV-Vis spectra were obtained using a Perkin Elmer Lambda 35 single-beam spectrophotometer, operating over a wavelength range of 200 to 900 nm. The program used to plot the graphs is WinLab Data Processor. The obtained data were utilized to determine the band gap energy of synthesized materials by constructing a Tauc plot using OriginLab software.

Picture 3.3. UV-Vis Spectrophotometer: Perkin Elmer Lambda 35.

4. RESULTS AND DISCUSSION

4.1. The Efficacy of the Sol-Gel Technique for Synthesizing $Mg_{3-x-y}Zn_xM_y/Al_1$ LDH and the Impact of Concentration Variations

This sol-gel technique facilitated the fabrication of the desired double metal-substituted $Mg_{3-x-y}Zn_xM_y/Al_1$ layered double hydroxide, where the magnesium (Mg) was partially replaced by two different metal cations (Zn and Ni/Co) and aluminum (Al), resulting in the targeted compositional ratios.

In the layered double hydroxides (LDHs), the precursors that contain nitrate (NO_3^-) or chloride (Cl^-) are the most appropriate for the ion exchange process. The LDH precursor containing carbonate anions was formed during the sol-gel synthesis process [37]. Whereas the carbonate anions are firmly integrated within the interlayer spaces of the LDH composition and typically do not undergo direct anion exchange [38][39].

In the synthesis of $Mg_{3-x-y}Zn_xM_y/Al_1$ LDH, varying the relative amounts of Mg, Ni and Co can lead to the crystal structure change, layer stacking, and the distribution of cations within the layers [40][41]. These structural modifications can then influence the electronic, optical, and magnetic properties of the LDH material, making it suitable for a wide-ranging application [42][43].

Explanation the color change of $Mg_{3-x-y}Zn_xM_y/Al_1$ LDH in response to concentration variations necessitate considering the interplay between the LDH structure and external influencing factors. The concentration of LDHs can significantly impact their properties. Specifically, an increase in the concentration of $Mg_{3-x-y}Zn_xM_y/Al_1$ LDHs can result in deeper colors [44]. The increase in cobalt concentration resulted in a more intense pink hue in the sample, while increasing the nickel concentration resulted in an enhancement of the green color in the sample. This alteration in color is attributed to the morphological variations that LDHs undergo under different conditions [45].

The morphologies of LDH materials can be altered by adjusting factors such as the Mg^{2+}/M^{2+} molar ratio, which can subsequently influenced the optical properties of the LDHs. Alteration in the molar ratio can lead to variations in the size, shape, and crystallinity of the LDH particles, ultimately influencing their color [46].

Figures (4.1–4.9) illustrate the three distinct sample concentrations of synthesized materials obtained at each stage of the Mg_{3-x-y} $Zn_{\times}Ni_{y}/Al_{1}$ LDH synthesis process.

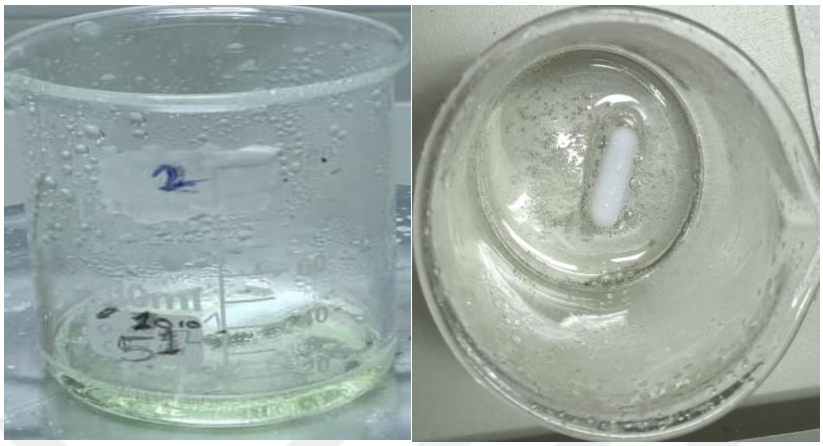

Figure 4.1. Wet gel of Mg_{3-x-y} $Zn_{\times}Ni_{y}/Al_{1}$ after hydrolysis and condensation.

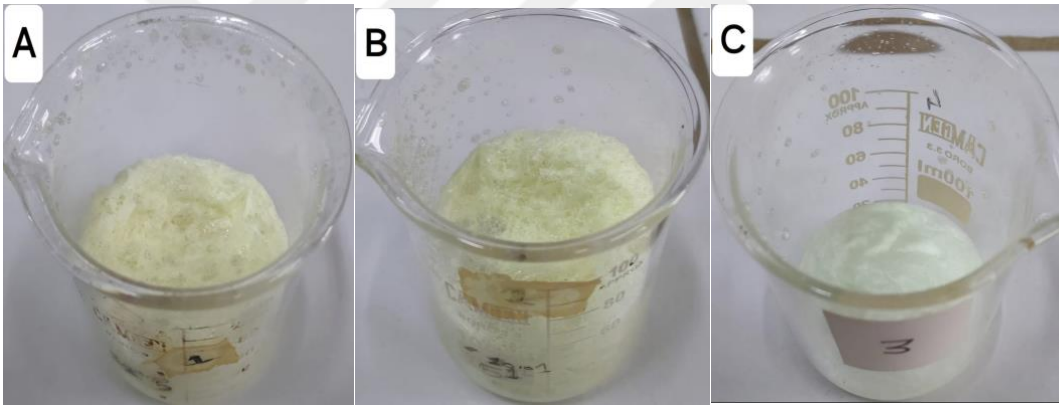

Figure 4.2. Dried gel of A) $Mg_{2.89}$ $Zn_{0.1}$ $Ni_{0.01}$ Al_{1}**,** B) $Mg_{2.87}$ $Zn_{0.1}$ $Ni_{0.03}$ Al_{1},C) $Mg_{2.85}$ $Zn_{0.1}$ $Ni_{0.05}$ Al_{1} obtained after being heated at 150ºC for 24 hours.

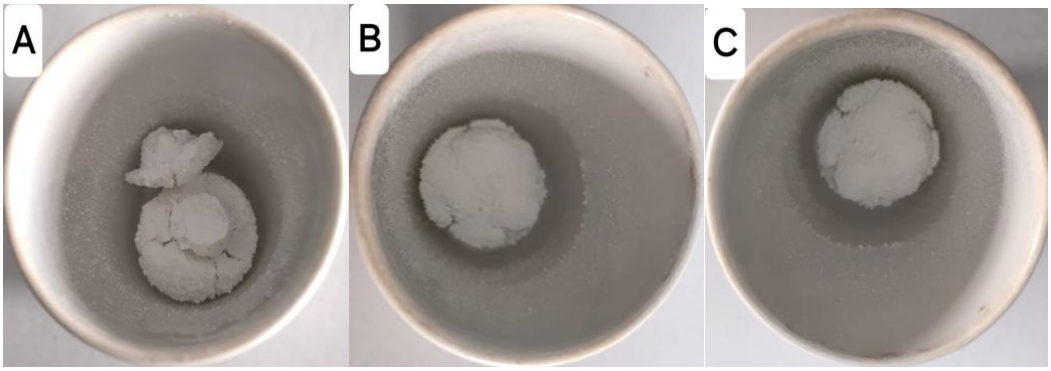

Figure 4.3. Mixed metal oxides (MMO) of A) $Mg_{2.89}$ $Zn_{0.1}$ $Ni_{0.01}$ Al_{1}, B) $Mg_{2.87}$ $Zn_{0.1}$ $Ni_{0.03}$ Al_{1}, C) $Mg_{2.85}$ $Zn_{0.1}$ $Ni_{0.05}$ Al_{1} obtained after being heated at 650ºC for 4 hours.

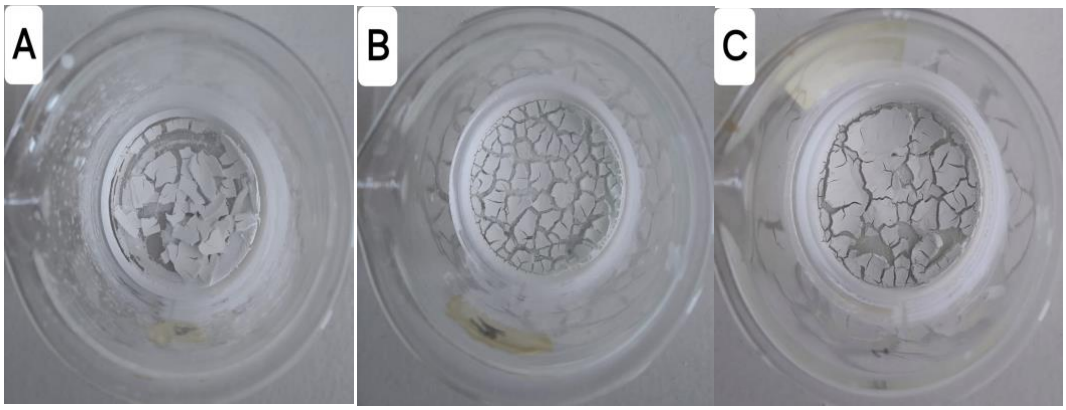

Figure 4.4. A) MgZnNi/Al LDH1, B) MgZnNi/Al LDH2, C) MgZnNi/Al LDH3.

Figure 4.5. MgZnNi/Al LDH powder after grinding.

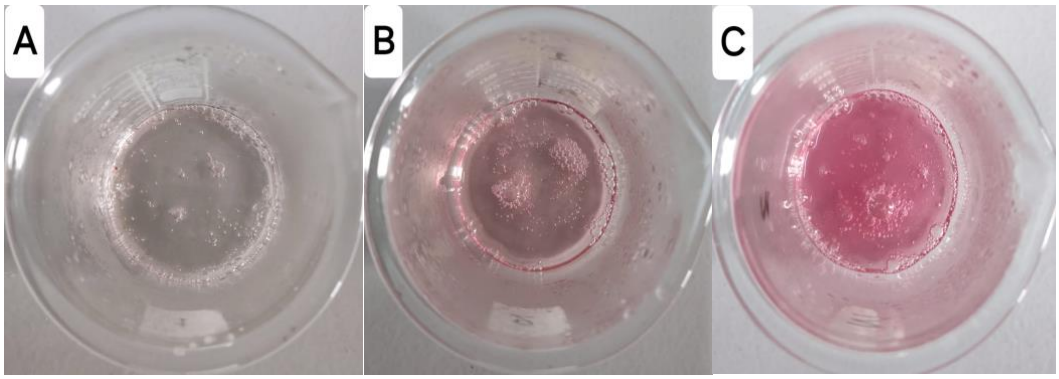

Figure 4.6. Wet gel of A) $Mg_{2.89}$ $Zn_{0.1}$ $Co_{0.01}$ Al_1, B) $Mg_{2.87}$ $Zn_{0.1}$ $Co_{0.03}$ Al_1, C) $Mg_{2.85}$ $Zn_{0.1}$ $Co_{0.05}$ Al_1.

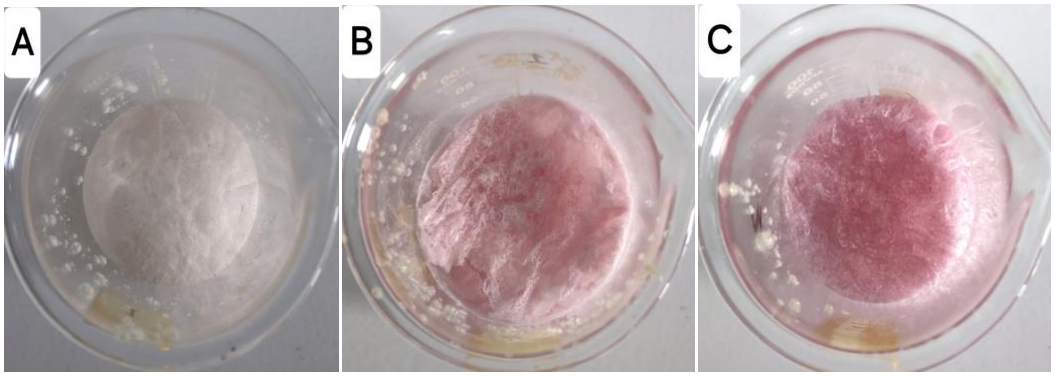

Figure 4.7. Dried gel of A) $Mg_{2.89}$ $Zn_{0.1}$ $Co_{0.01}$ Al_1, B) $Mg_{2.87}$ $Zn_{0.1}$ $Co_{0.03}$ Al_1, C) $Mg_{2.85}$ $Zn_{0.1}$ $Co_{0.05}$ Al_1.

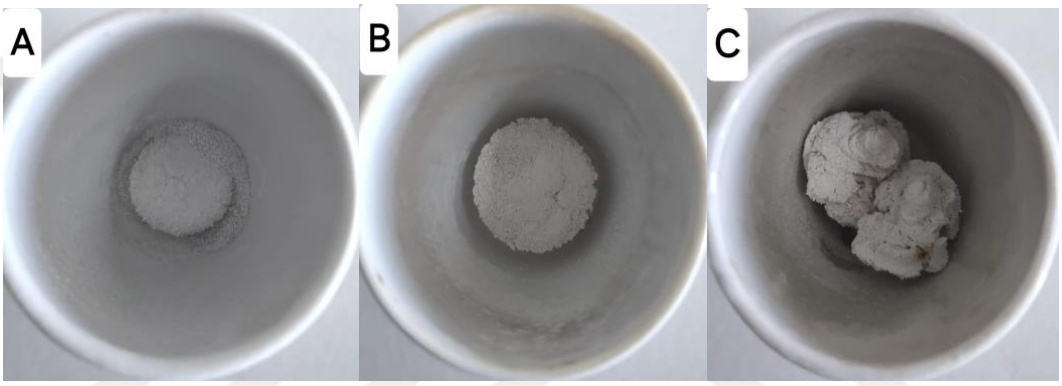

Figure 4.8. Mixed metal oxides of A) $Mg_{2.89}$ $Zn_{0.1}$ $Co_{0.01}$ Al_1, B) $Mg_{2.87}$ $Zn_{0.1}$ $Co_{0.03}$ Al_1, C) $Mg_{2.85}$ $Zn_{0.1}$ $Co_{0.05}$ Al_1.

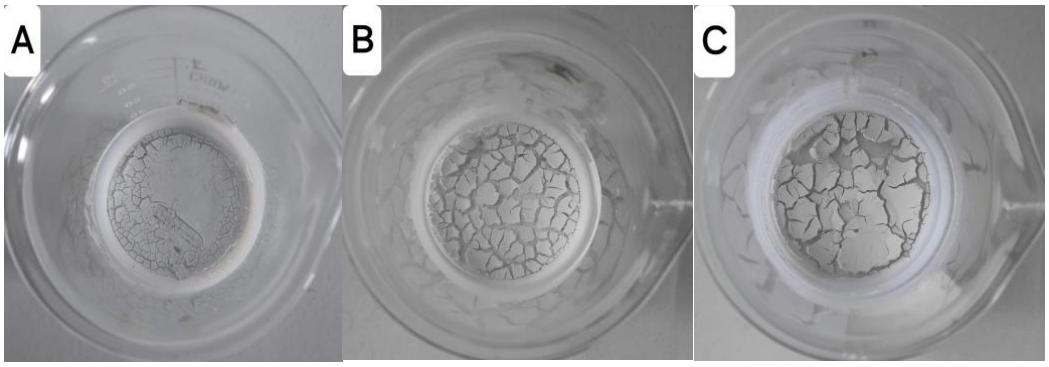

Figure 4.9. A) MgZnCo/Al LDH1, B) MgZnCo/Al LDH2, C) MgZnCo/Al LDH3.

4.2. X-Ray Diffraction (XRD) Analysis

To conduct a thorough analysis of the structural variations in $Mg_{3-x-y}Zn_xM_y/Al_1$ layered double hydroxide during its synthesis, MgZnCo/Al LDH1 was chosen as a representative case study. In this regard, X-ray diffraction analysis was conducted on xerogel and metal mixed oxide (MMO) samples. As shown in Figures (4.10 and 4.11) The X-ray diffraction (XRD) patterns obtained from the MgZnCo/Al LDH1 sample, which was subjected to a temperature of 650°C, show the formalization of mixed metal oxides from the precursor gel during the heating process. The XRD patterns exhibit two distinct peaks, in particular the sharp peak between 40-50 2θ° which corresponds to the existence of a mixed metal oxide (MMO) phase. These peaks are completely correlated as to that of magnesium oxide (JCPDS No. 96-100-0054) [47]. A reasonably crystalline magnesium oxide is formed. The high-temperature treatment of LDHs led to the water molecules removal in the interlayer (dehydration) creating anhydrous phases, and also minimized the anions that exist there for charge balance maintenance. As a result, the hydroxyl groups ($^-$OH) are excluded from the brucite-like layers [48][49]. The xerogel sample did not show any clear or distinct signal in the analysis, as expected. Xerogels are highly porous, amorphous materials that often lack long-range order, making it challenging to obtain well-defined signals in analytical techniques such as X-ray diffraction or spectroscopic methods. The lack of a clear signal in the analysis was the predictable outcome for this type of sample.

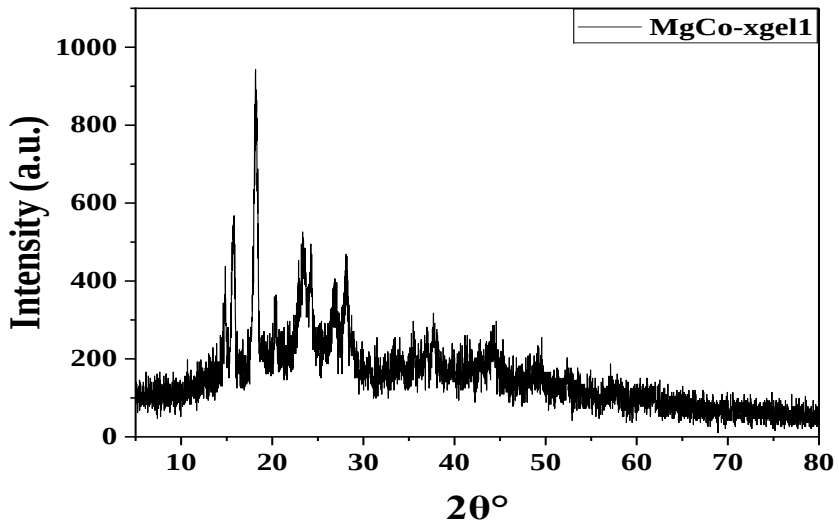

Figure 4.10. XRD pattern of MgZnCo/Al xerogel

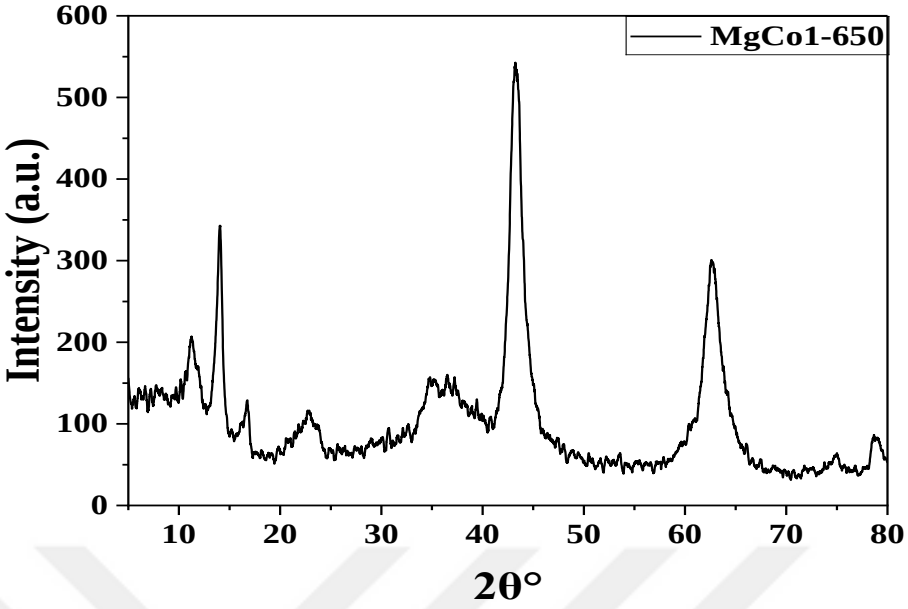

Figure 4.11. XRD pattern of MgZnCo/Al mixed metal oxides

The Figures shown below (4.12 and 4.13) illustrate the X-ray diffraction patterns for the three different concentrations of MgZnCo/Al LDH and MgZnNi/Al LDH. The similarity in the XRD patterns across the six samples suggests that they likely have a common structural backbone, despite potential variations in their specific compositions. The observed diffraction patterns were the characteristic d-lines that were often discussed in layered double hydroxide materials and literatures. The distinct diffraction peaks observed in the $Mg_{3-x-y}Zn_xM_y/Al_1$ LDH samples, particularly the two peaks around 60 2θ°, are indicative of the presence of the hydrotalcite phase, as identified by the (JCPDS No. 20-0700). The well-defined and intense nature of these peaks suggests the presence of pure, highly ordered crystalline material. These observations indicate that the sample has a layered double hydroxide structure with different metal ions have substituted into the layers to varying amounts.

The X-ray diffraction (XRD) data reveals a higher average intensity for the Nickel LDH samples (average of 2300 a.u) compared to the Cobalt LDH samples (average of 1800 a.u). This observation suggests an enhanced degree of crystallinity in the Nickel LDH samples [50], indicating a more organized arrangement of atoms within a well-defined crystalline structure [51]. This is due to the nickel's smaller

atomic radius compared to cobalt, resulting in a higher level of structural arrangement within the hydroxide layers.

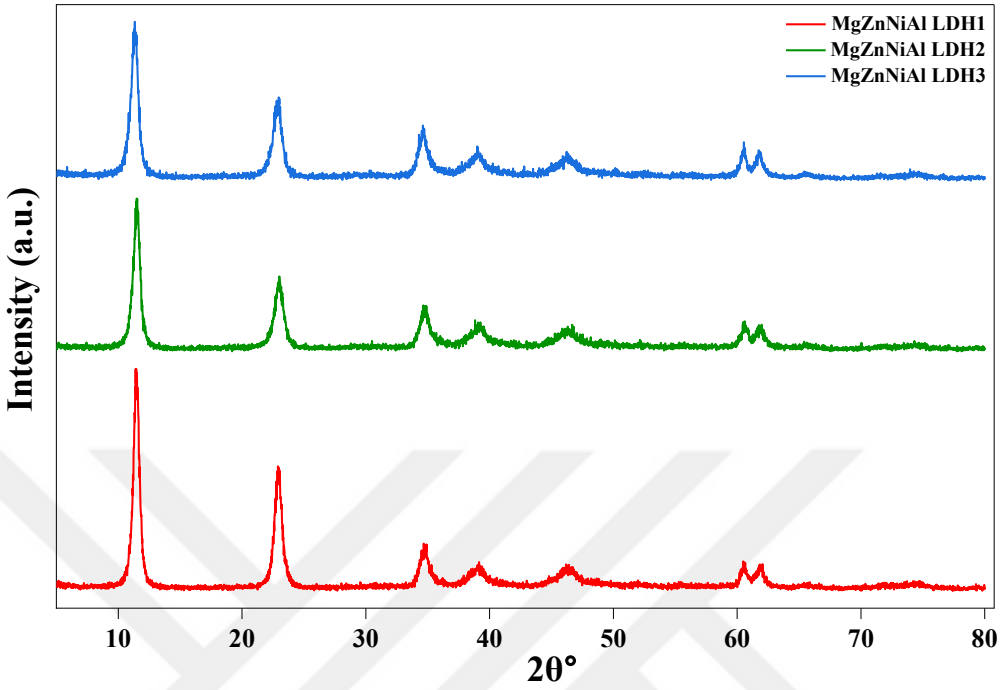

Figure 4.12. XRD Patterns of MgZnNi/Al LDH.

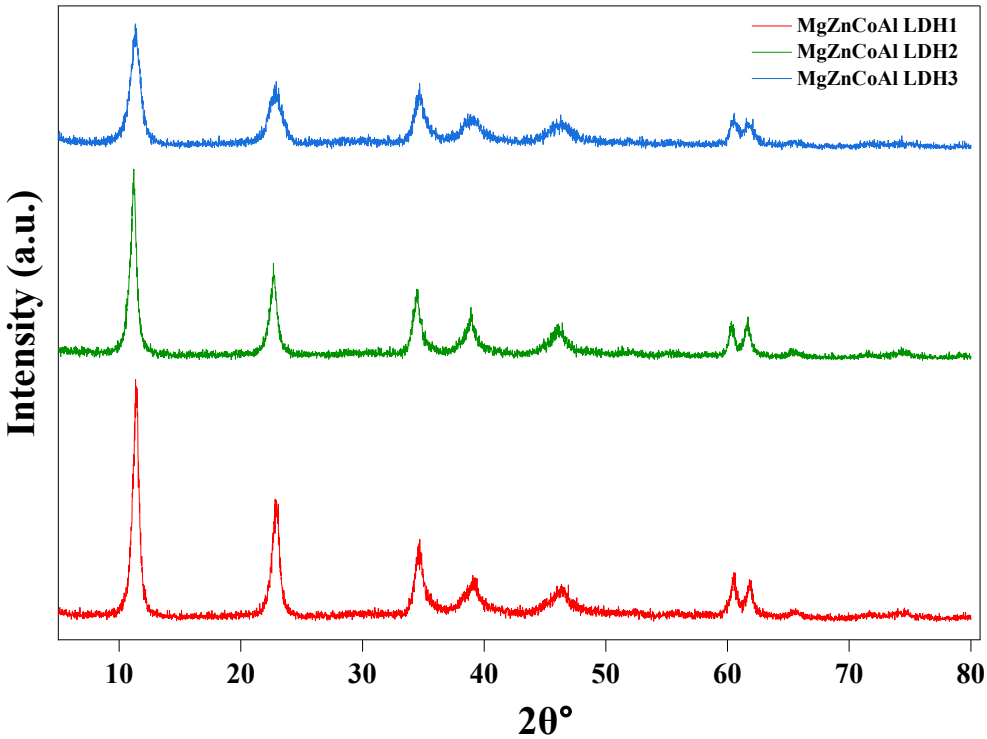

Figure 4.13. XRD Patterns of MgZnCo/Al LDH.

4.3. Fourier-Transform Infrared Spectroscopy (FT-IR) Analysis

The FT-IR spectra of the xerogel as shown in Figures (4.14 and 4.15) exhibit an absorption peak near to 3459 cm^{-1}, this peak is abroad which corresponds ^{-}OH group stretching vibration of the metal hydroxide, while the sharp strong band around 1366 cm^{-1} corresponds NO^{3-} groups. Figures (4.16 and 4.17) represent the FT-IR spectra of mixed metal oxide samples. The magnesium oxide nanoparticles exhibit a chemisorption phenomenon where H_2O and CO_2 molecules are adsorbed onto their surfaces. A wide peak is observed around 3435 cm^{-1}, indicating the stretching vibrations of O-H in the water molecules adsorbed on the MgO layer surface [52]. In addition, bands around 1737 cm^{-1} suggest the bending vibrations of these adsorbed water molecules at the surface [53], while a peak corresponding to NO^{3-} appears at 1366 cm^{-1} [54]. Furthermore, the low-frequency peaks between 450-800 cm^{-1} in both xerogel and MMO spectra are potentially associated with the stretching of metal-oxygen bonding [55].

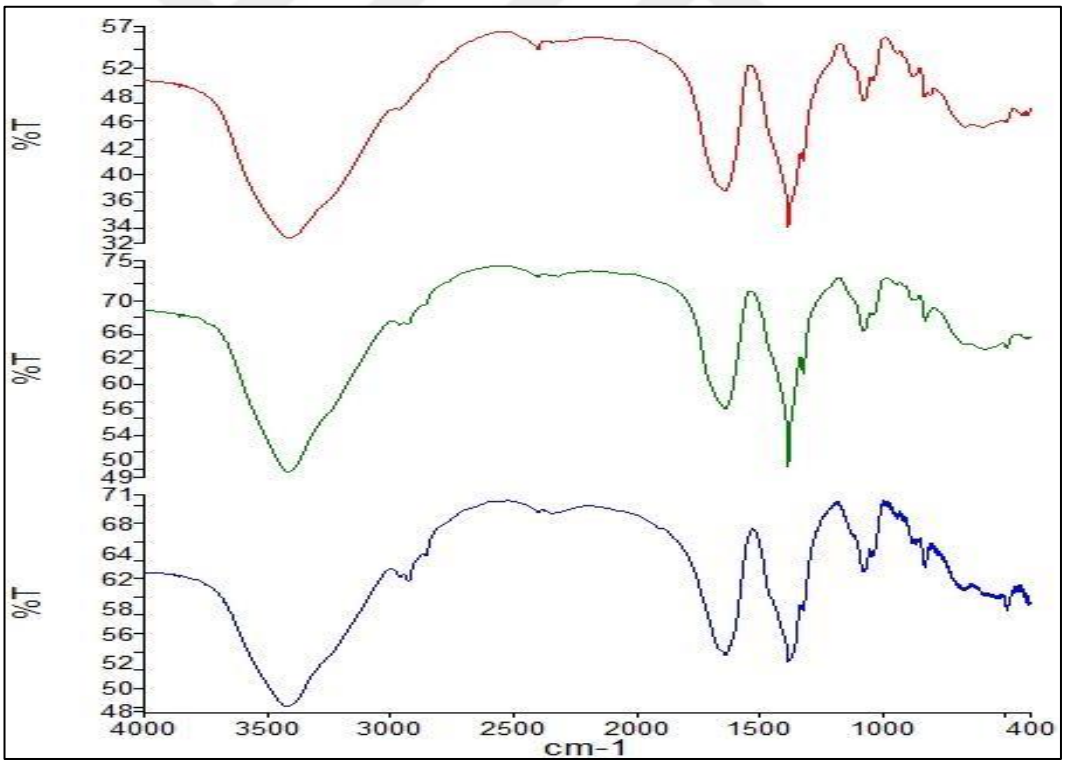

Figure 4.14. IR spectra of MgZnNi/Al xerogel.

Where the red line symbolizes the first concentration, the green line symbolizes the second concentration, and the blue line symbolizes the third concentration.

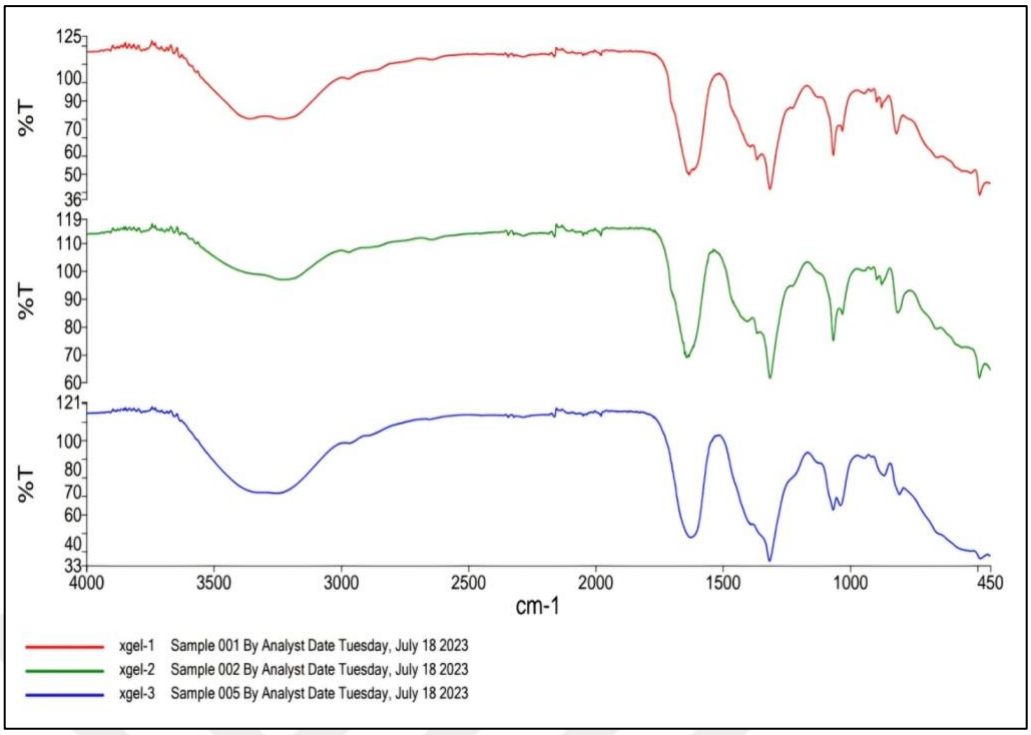

Figure 4.15. IR spectra of MgZnCo/Al xerogel.

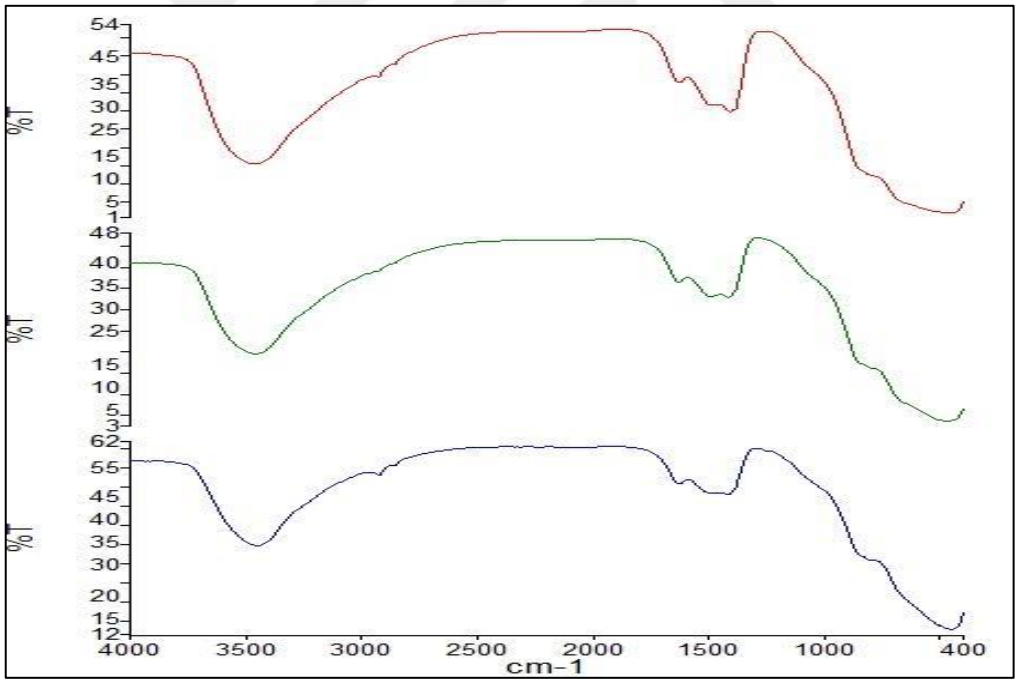

Figure 4.16. IR spectra of MgZnNi/Al Mixed Metal Oxides (MMO).

Where the red line symbolizes the first concentration, the green line symbolizes the second concentration, and the blue line symbolizes the third concentration.

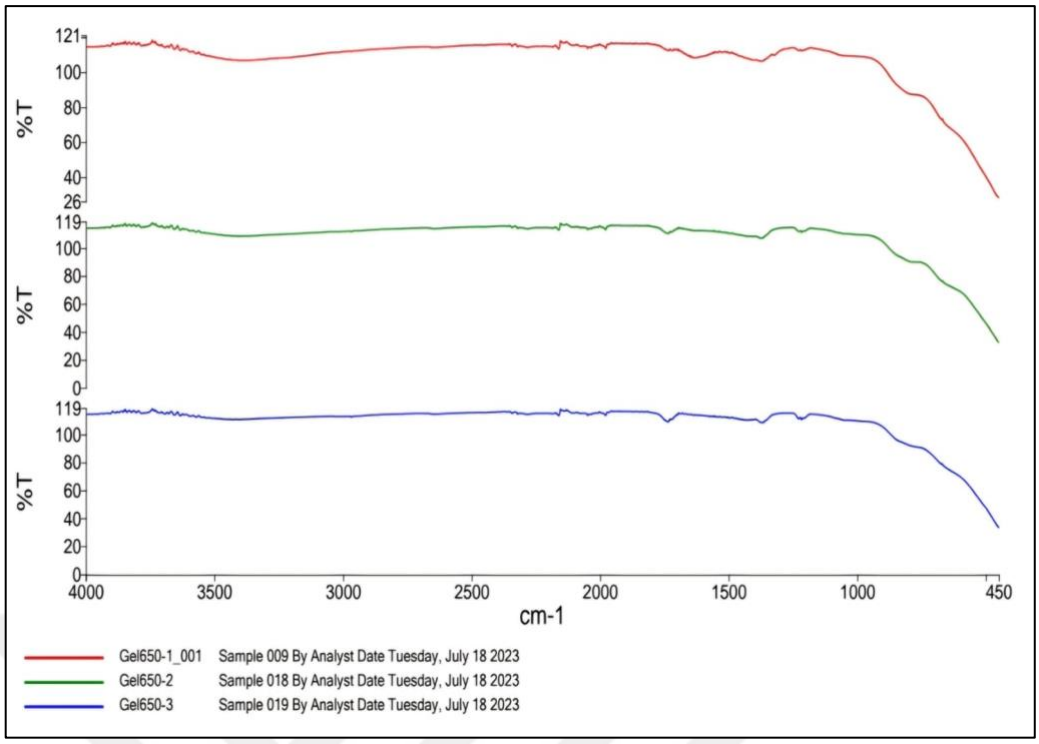

Figure 4.17. IR spectra of MgZnCo/Al Mixed Metal Oxides (MMO).

With reference to Figures (4.18 and 4.19), the FT-IR spectra of MgZnNi/Al-NO_3 and MgZnCo/Al-NO_3 reveal several considerable absorption bands. A strong and broad band appeared at 3459.8, 3457.7 and 3436.3 cm^{-1} respectively in MgZnCo/Al LDH samples IR spectra. As well as, for MgZnCo/Al LDH comparable high-intensity, broad peaks appeared approximant at 3490 cm^{-1}. These observed peaks correspond to hydroxyl groups (OH^-) stretching vibrations in the brucite-like layer, likewise for the vibrations caused by the stretching of oxygen-hydrogen bonding in interlayer water molecules. Moreover, a strong, sharp peak at 1366 cm^{-1} is associated with the v_3 vibrational mode with D_3h symmetry in the nitrate groups (NO_3^-) [56], as shown in Figure (4.20).

The peak near to 1651 cm^{-1} indicates the bending vibrations of water molecules in the interlayer. Additionally, few absorption peaks between 450 and 750 cm^{-1} are associated with stretching modes of metal-oxide bonding. These peaks have low intensity and low frequency [56]. Furthermore, the presence of H_2O-NO_3 bridging vibrations was inferred from the shoulder peak around 2900 cm^{-1} [57]. Presented in Figure (4.18 and 4.19), the red line symbolizes the first concentration ($Mg_{2.89}Zn_{0.1}M'_{0.01}$), the green line symbolizes the second concentration

($Mg_{2.87}Zn_{0.1}M'_{0.03}$), and the blue line symbolizes the third concentration ($Mg_{2.85}Zn_{0.1}M'_{0.05}$), where M' is Nickle or Cobalt.

The diverse vibrational modes of the various functional groups and bonds, as well as their approximate absorption ranges in MgZnNi/Al LDH and MgZnCo/Al LDH, are visually depicted in Figure (4.20).

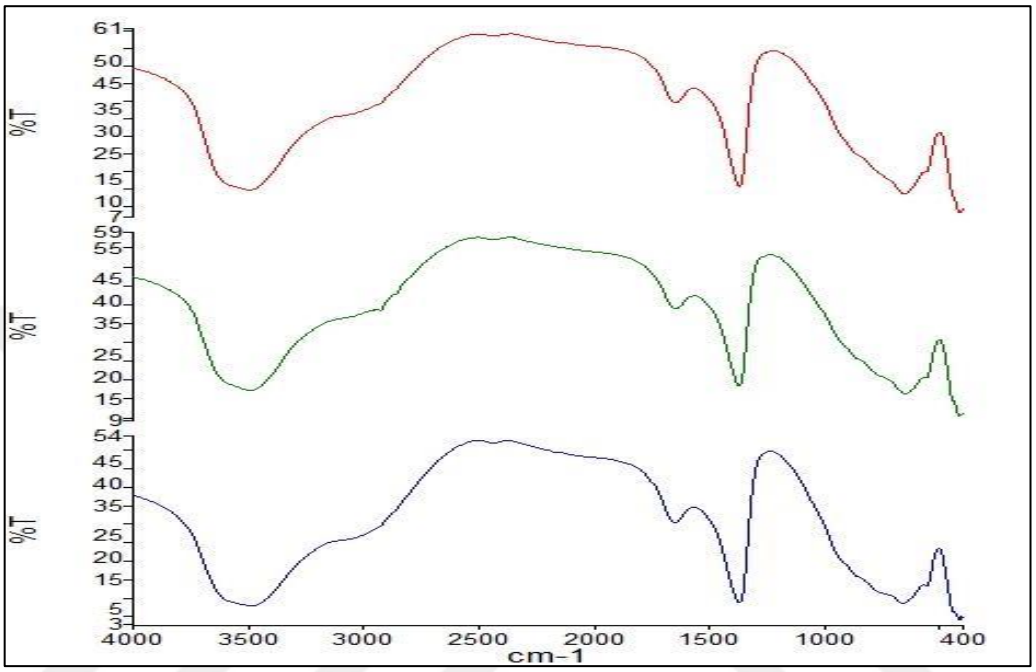

Figure 4.18. IR spectra of MgZnNi/Al LDH.

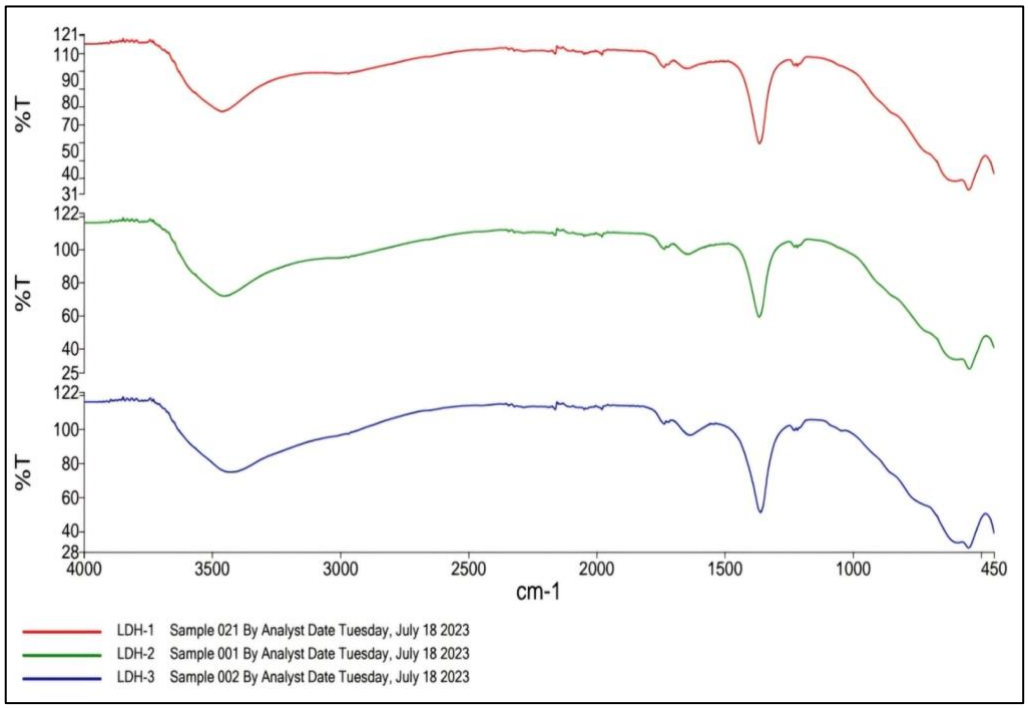

Figure 4.19. IR spectra of MgZnCo/Al LDH.

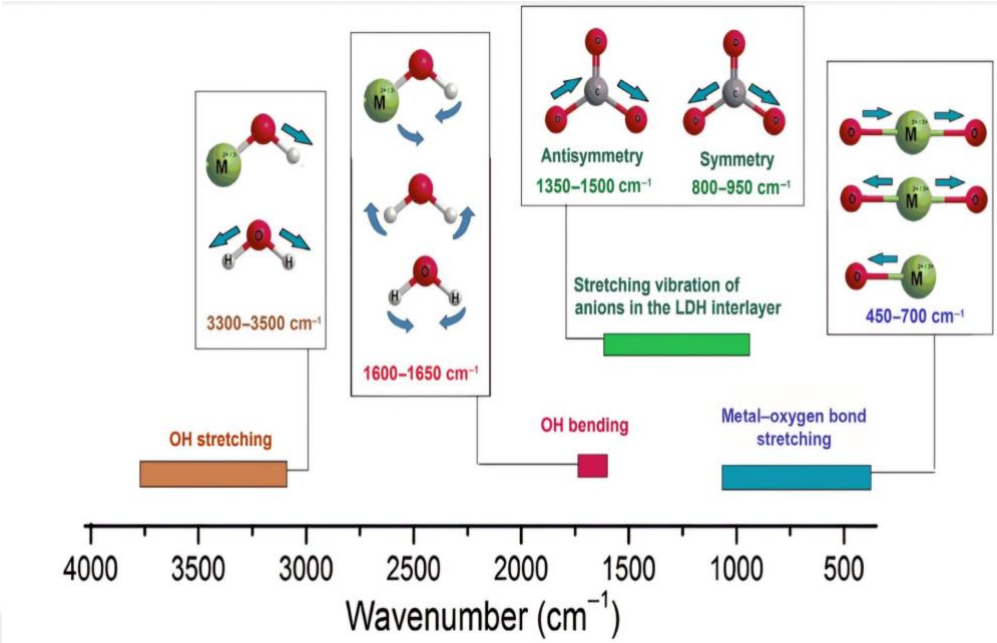

Figure 4.20. Illustration of the different vibrational modes in MgZnM/Al-NO_3 LDH.

4.4. UV-Vis absorbance spectroscopy and Diffuse Reflectance Spectroscopy (DRS) Analysis

To thoroughly investigate the optical properties of $Mg_{3-x-y}Zn_xM_y/Al_1$ layered double hydroxide during its synthesis, MgZnNi/Al LDH was selected as a representative case study. In this context, UV-Vis absorbance spectroscopy and diffuse reflectance spectroscopy were performed on xerogel samples and metal mixed oxide samples (MMOs), as well as on the nickel LDH samples. As shown in Figures (4.21 to 4.26).

UV-Vis absorption spectra of magnesium hydroxide and magnesium oxides are recorded within the range of 200-400 nm as shown in Figures (4.21-4.24). The $Mg(OH)_2$ shows a sharp absorption peaks around 255 and 332 nm [58], while an intense peaks appeared around 260 and 387 nm confirming the presence of MgO [59]. The UV-Vis data analysis of MMO demonstrated a direct correlation between concentration and absorbance. Notably, the third concentration exhibited a significantly higher absorbance compared to the other concentrations.

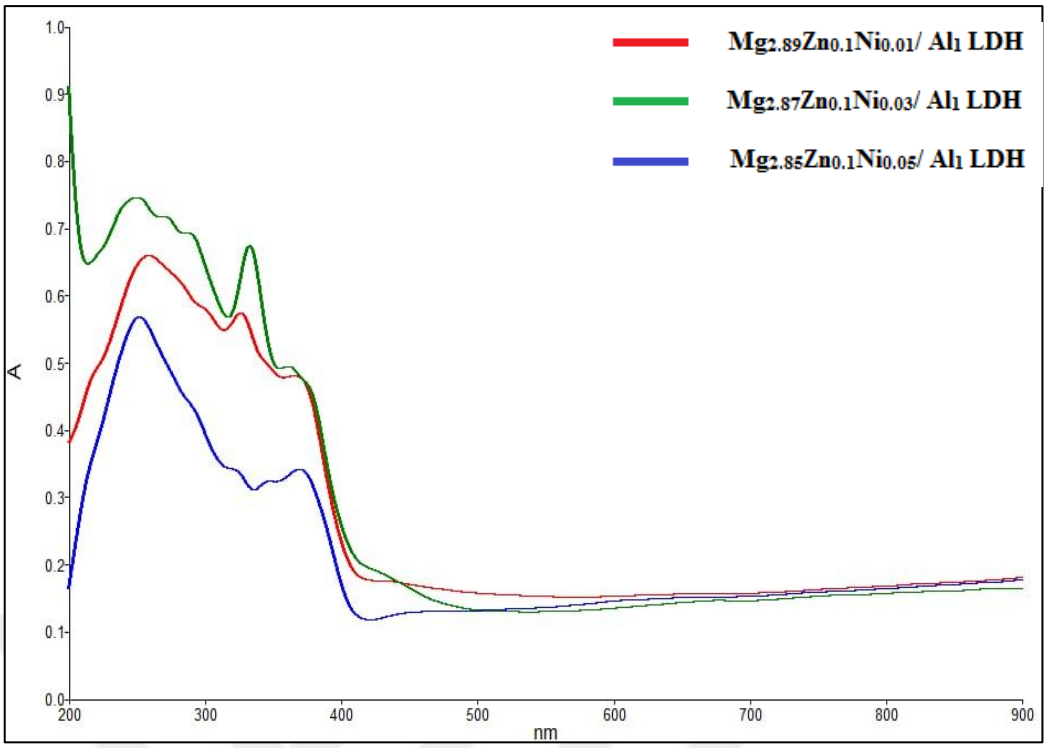

Figure 4.21. UV-Vis absorbance spectra of MgZnNi/Al Xerogel.

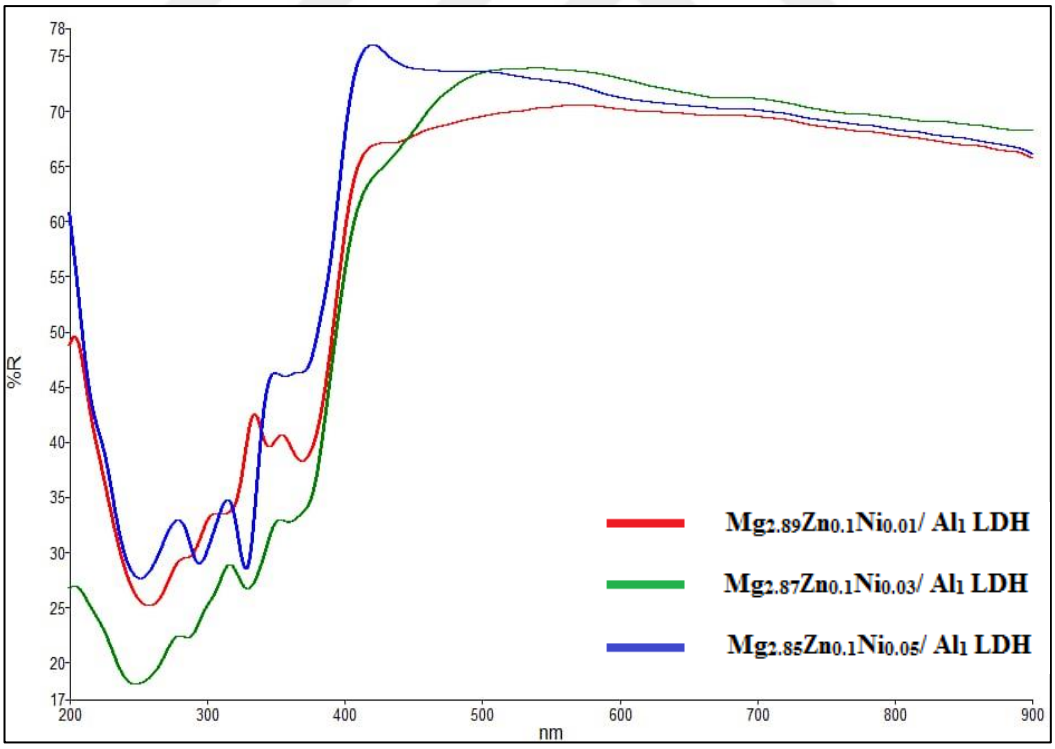

Figure 4.22. UV-Vis reflectance spectra of MgZnNi/Al xerogel.

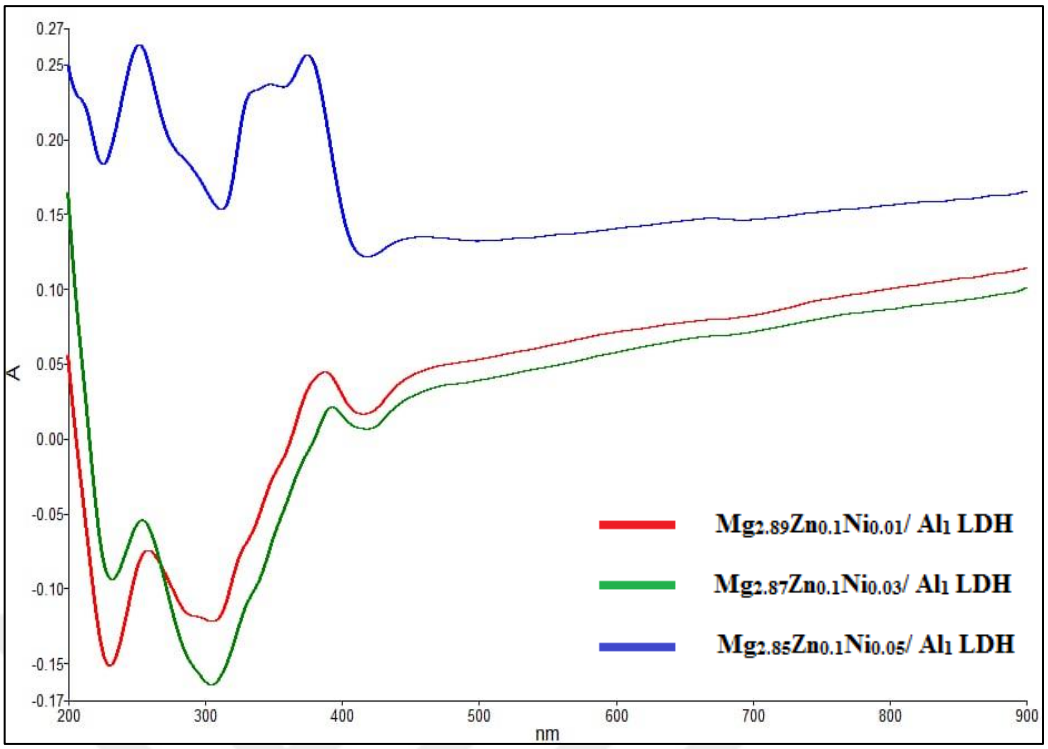

Figure 4.23. UV-Vis absorbance spectra of MgZnNi/Al MMO.

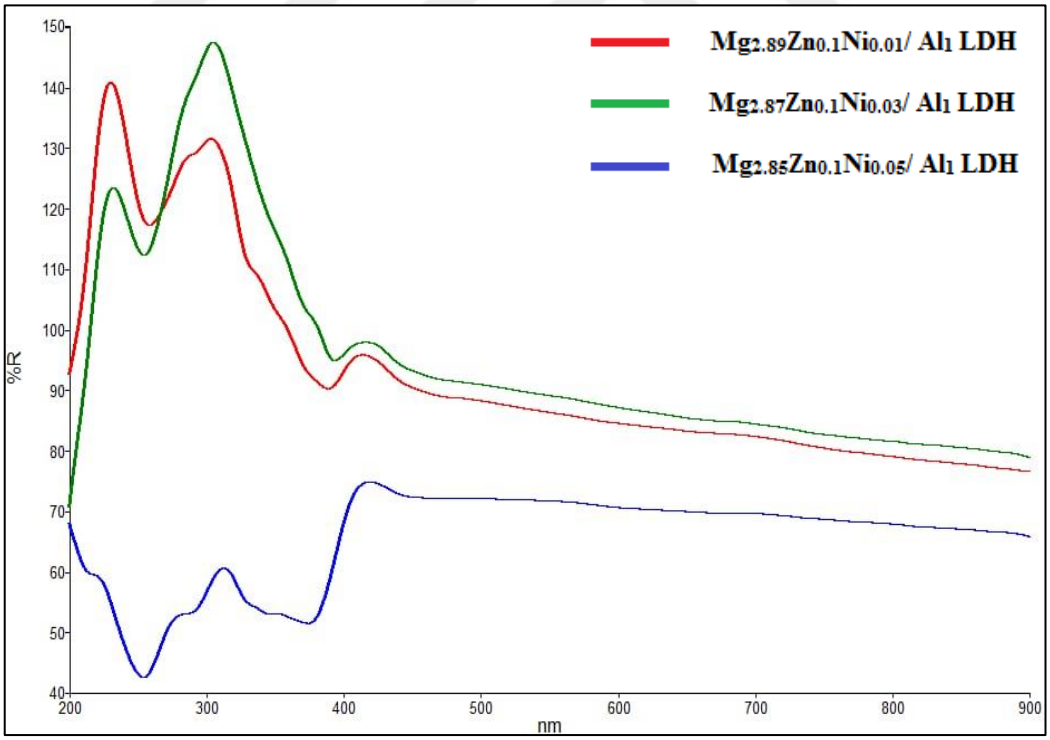

Figure 4.24. UV-Vis absorbance spectra of MgZnNi/Al MMO.

The distinct peaks that attributed to the pi-pi transition of zinc and nickel metals during the metal substitution process in MgZnNi/Al LDH [60] are discernible in the ultraviolet-visible absorbance spectra (presented in Figure

4.24) and UV-Vis reflectance spectra (shown in Figure 4.25). Despite being a transition element known for exhibiting color, nickel's absorbance peaks were observed within the ultraviolet spectrum, specifically between 200 and 400 nanometer [61]. This observation corroborates the notion that nickel exhibits a high degree of structural arrangement within its hydroxide layers [62]. MgZnNi/Al LDH samples show sharp and intense absorption peaks respectively around 258.9 and 375.8 nm for MgZnNi/Al LDH1, 258.8 and 368.7 nm for MgZnNi/Al LDH2, 258.8 and 375 nm for MgZnNi/Al LDH3. As well as, sharp and intense reflection peaks showed respectively around 260.3 and 377.1 nm for MgZnNi/Al LDH1, 259.8 and 367 nm for MgZnNi/Al LDH2, 259.2 and 377.8 nm for MgZnNi/Al LDH3.

Based on the UV-Vis data, it is evident that MgZnNi/Al LDH2 demonstrates a significantly higher absorbance compared to other samples, indicating a potentially higher concentration of LDH structural within that particular sample. Meanwhile, it shows a redshift towards longer wavelengths on MgZnNi/Al LDH1 and MgZnNi/Al LDH3 peaks.

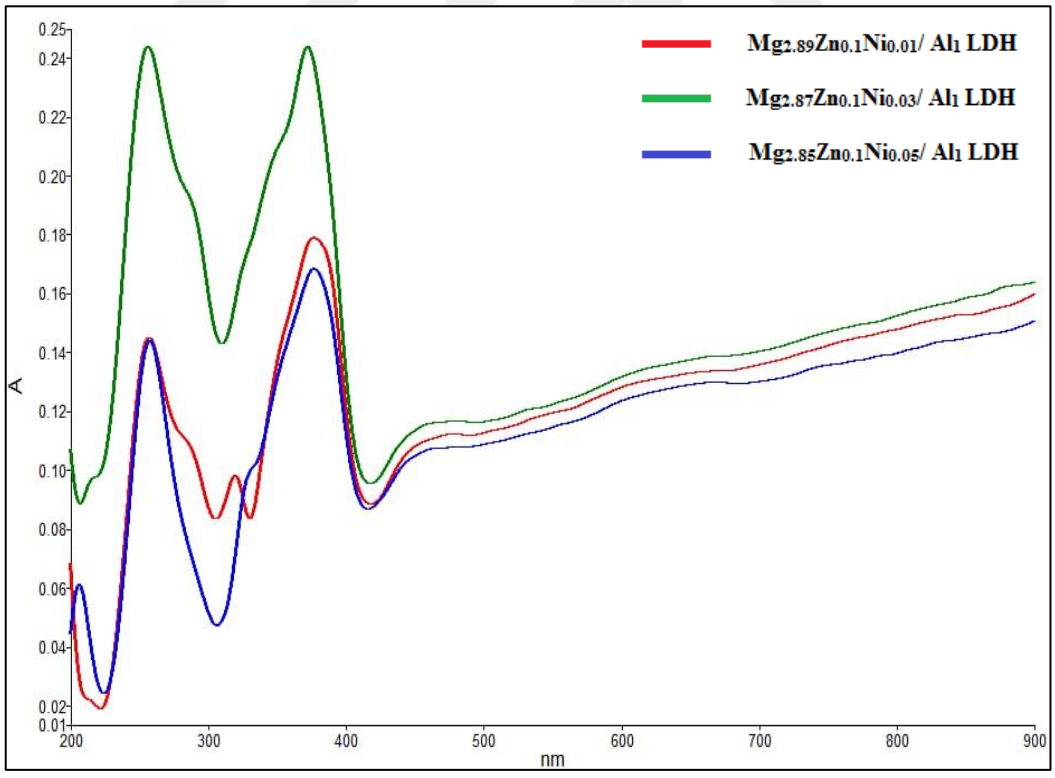

Figure 4.25. UV-Vis absorbance spectra of MgZnNi/Al LDH.

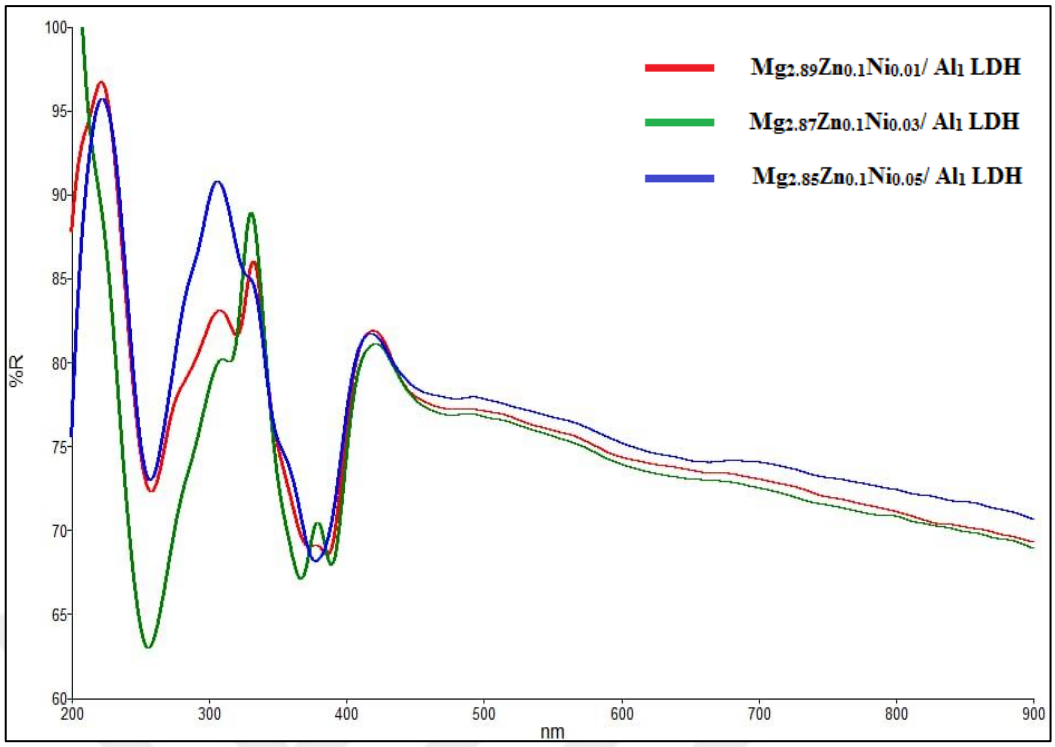

Figure 4.26. UV-Vis reflectance spectra of MgZnNi/Al LDH.

The UV-Vis absorbance and reflectance spectra of MgZnCo/Al LDH were acquired over the wavelength range of 200–900 nm, as shown in Figures 4.27 and 4.28, respectively. The absorption spectra reveal that Co-LDH1, which has the lowest cobalt concentration, exhibits the highest absorbance. This is followed by $Mg_{2.85}Zn_{0.1}Co_{0.05}/Al_1$ and $Mg_{2.87}Zn_{0.1}Co_{0.03}/Al_1$, indicating that lower cobalt concentrations contribute to greater light absorption. Conversely, the reflectance spectra show an inverse relationship, where Co-LDH1 reflects less light compared to the other samples. This suggests that the materials with higher absorbance have lower reflectance, consistent with the inverse relationship between absorption and reflectance properties.

This observation also suggests effective substitution of transition metals into the host materials, as evidenced by the undetectable peaks in the visible region of the UV-Vis absorbance and reflectance spectra. This indicates that the transition metals are well-integrated and do not introduce additional visible light absorption features. Additionally, the low concentration of d- metal ions might contribute to the lack of observable peaks in the visible range, suggesting that their presence does not significantly alter the optical properties in that region.

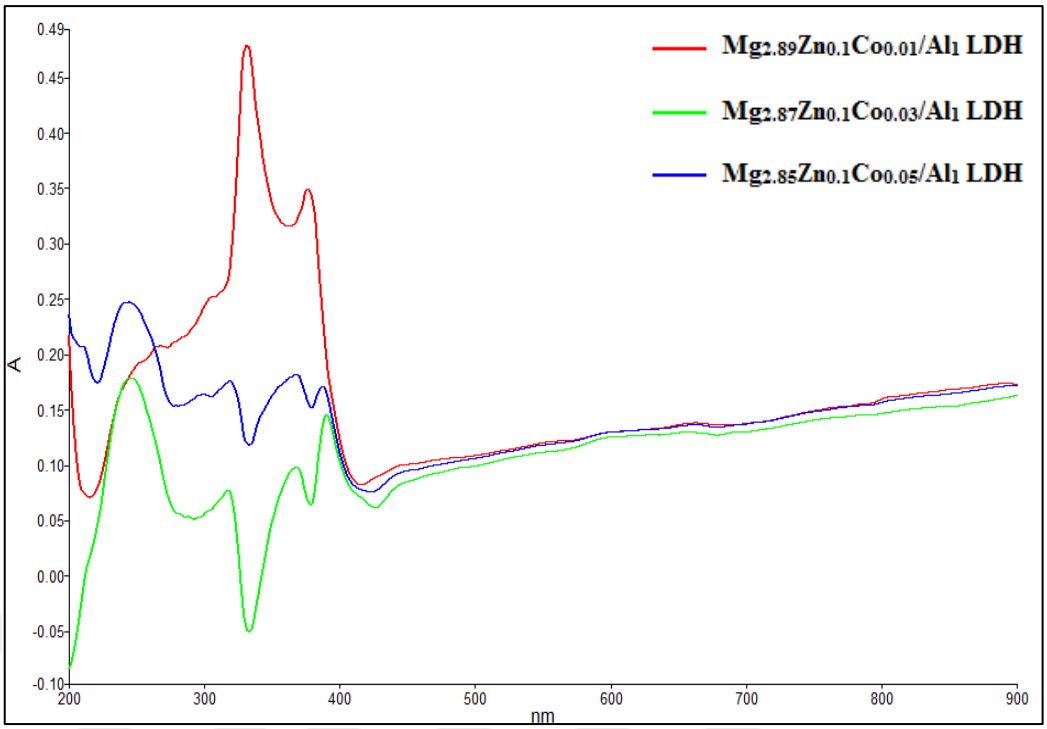

Figure 4.27. UV-Vis absorbance spectra of MgZnCo/Al LDH.

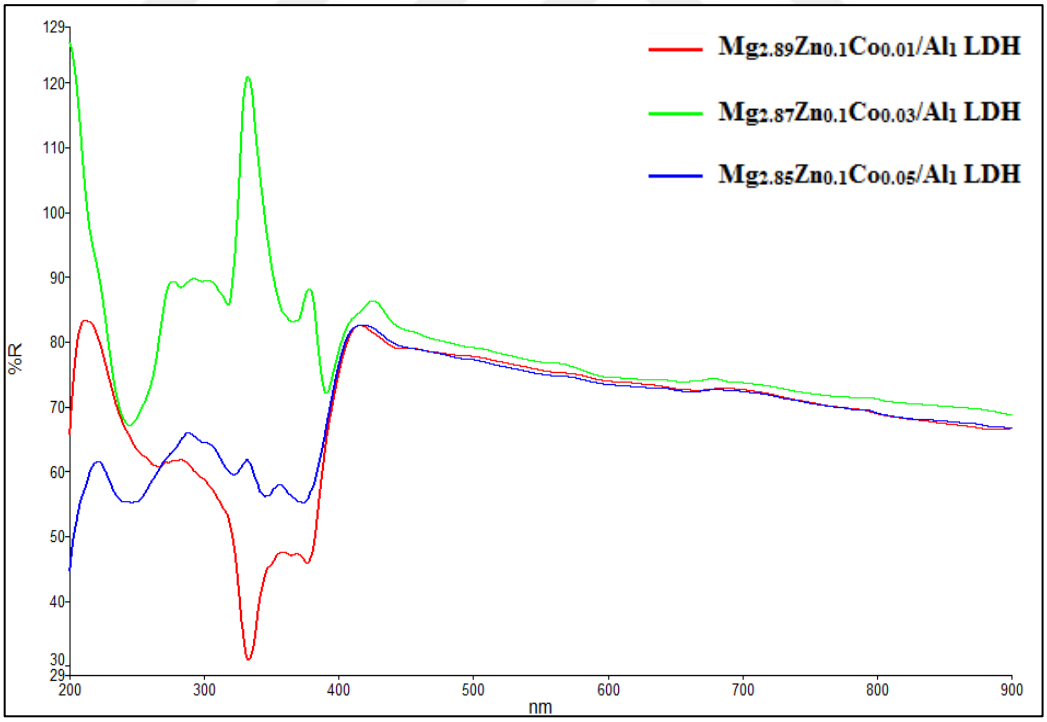

Figure 4.28. UV-Vis reflectance spectra of MgZnCo/Al LDH.

4.5. Structural and Optical Properties

By utilizing the obtained UV-Visible data and XRD data, several structural and optical properties were meticulously calculated and are presented in (Tables 4.1 and 4.2) These properties include lattice parameters (a and c), crystallite sizes (D), microstrain (ε), positions and displacements of atoms (u), unit cell volume (v), band gap, and dielectric constant (*κ).*

Table 4.1. Values of lattice parameters (a and c), crystallite sizes (D) and microstrain (ε).

Sample Name	D (nm)	c (Å)	a (Å)	Ɛ
MgZnNiAl LDH1	9.14	23.130	3.0555	16.5417
MgZnNiAl LDH2	8.14	23.090	3.0534	18.9062
MgZnNiAl LDH3	8.58	23.440	3.0574	19.1071
MgZnCoAl LDH1	8.89	23.330	3.0570	18.0982
MgZnCoAl LDH2	9.86	23.750	3.0645	15.7568
MgZnCoAl LDH3	6.85	23.420	3.0571	23.9041

Table 4.2. Values of volume of the unit cell (v), positions and displacements of atoms (u), band gap and dielectric constant (*κ).*

Sample Name	V ($Å^3$)	U	Band gap (eV)	Dielectric Constant
MgZnNiAl LDH1	187.0343	72.2395	3.054	7.9165
MgZnNiAl LDH2	186.4749	72.0242	3.050	7.9223
MgZnNiAl LDH3	189.7524	73.2857	3.042	7.9340
MgZnCoAl LDH1	188.8321	72.9315	3.054	7.9165
MgZnCoAl LDH2	193.1662	74.5997	3.068	7.8964
MgZnCoAl LDH3	189.5660	73.2140	3.062	7.9050

The XRD data obtained for MgZnNi/Al LDH samples and MgZnCo/Al LDH samples were utilized to calculate the crystallite size and lattice parameters (given in Table 4.1). The Debye-Scherrer equation was used to determine the average crystallite size [63][64]. The Debye-Scherrer equation is:

$$D = \frac{K\lambda}{\beta \mathrm{Cos}\theta}$$

Where D denoted the crystallite size, K is the Scherrer constant which equal to 0.9, λ is the X-ray wavelength (1.5406Å), θ is the Bragg's angle and β represents the full width at half maximum (FWHM) [65]. The crystallite size of $Mg_{3-x-y}Zn_xM_y/Al_1$ layered double hydroxide samples varied between 6.8 and 9.9 nm. Generally, the average crystallite size of MgZnCo/Al LDH samples was larger than that of MgZnNi/Al LDH samples, which is in high alignment with the XRD data. This is consistent with the larger atomic radius of cobalt. The largest crystallite size observed for MgZnNiAl LDH was 9.14, while that for MgZnCoAl LDH was 9.86, confirming the formation of nanosized materials. LDHs with highest crystallite size exhibit improved stability and enhanced mechanical properties such as hardness and strength [66][67]. Furthermore, the measurements did not reveal any consistent correlation between the change in concentration and the average crystallite size of $Mg_{3-x-y}Zn_xM_y/Al_1$ LDH.

The lattice parameters (a and c) of $Mg_{3-x-y}Zn_xM_y/Al_1$ LDH samples were examined by using Bragg's equation. The lattice constants were calculated by analyzing the positions of X-ray peak associated with lattice plane reflections (hkl) [70] , where, the lattice constant for a is a = b = 2d, while for c is c = 3d.

$$\frac{1}{d^2} = \frac{3}{4}\left(\frac{h^2 + hk + k^2}{a^2}\right) + \frac{l^2}{c^2}$$

As presented in (Table 4.1), the third concentration of Nickel in $Mg_{3-x-y}Zn_xNi_y/Al_1$ LDH (y = 0.05) corresponds to the highest values of a and c lattice parameters. In contrast, for $Mg_{3-x-y}Zn_xCo_y/Al_1$ LDH, the second concentration (y = 0.03) exhibits the maximum values of the a and c lattice parameters. Additionally, an inverse relationship was observed between the structural lattice parameters and the crystallite size. Furthermore, the atomic packing factor (c/a) was calculated using the a and c parameters' values and are listed in the (Table 4.3) below:

Table 4.3. Values of the atomic packing factor (c/a).

Sample Name	c/a
MgZnNiAl LDH1	7.5699
MgZnNiAl LDH2	7.5620
MgZnNiAl LDH3	7.6666
MgZnCoAl LDH1	7.6316
MgZnCoAl LDH2	7.7500
MgZnCoAl LDH3	7.6543

As illustrated in (Table 4.1), the microstrain values of $Mg_{3-x-y}Zn_xNi_y/Al_1$ LDH ranged from 16.5 to 19.2, while those of $Mg_{3-x-y}Zn_xCo_y/Al_1$ LDH ranged from 15.7 to 24. the microstrain value demonstrated a positive correlation with the increasing concentration of nickel, reaching its peak at the third concentration (y = 0.05) of the LDH. This observation suggests that the crystalline lattice experienced the highest degree of distortion at this specific concentration. Conversely, the microstrain value for cobalt increased when the cobalt concentration was increased from y = 0.01 to y = 0.05, but it dropped significantly to its lowest point at y = 0.03.

The unit cell volume, along with the positions of the atoms and their displacements were determined using the values of the a and c lattice parameters, as demonstrated in (Table 4.2). The volume of unit cell was calculated using the equation $v = \sqrt{3}/2.a^2c$, while the positions and displacements of the atoms were calculated using the equation $u = a^2/3c^2 + 0.25$ [68][69]. The maximum unit cell volume for MgZnNi/Al LDH was observed at the third concentration, while it was at the second concentration for MgZnCo/Al LDH. This indicates that the chemical pressure should be at a minimum at these specific concentrations [71]. With respect to the behavior of the positions of the atoms and their displacements, the atomic locality of the atoms was significantly and irregularly altered with an increase in the quantity of the substituting metals (nickel and cobalt), as presented in Table 4.2. Furthermore, the measurements indicated a similarity in the values of dielectric constant of all the examined LDH samples, which ranged from 7.89 to 7.94. Notably, the dielectric constant exhibited a positive correlation with the nickel

amount, reaching its peak at y = 0.05. Conversely, for cobalt, the dielectric constant generally decreased as the cobalt concentration increased, with its maximum value occurring at y = 0.01. These observations suggest that the highest electrical energy storage ability for MgZnNi/Al LDH and MgZnCo/Al LDH is achieved at their highest dielectric constant value.

The optical band gap energy of MgZnNi/Al LDH and MgZnCo/Al LDH at varying concentrations was computed using UV-Visible absorbance data. This were achieved using a Tauc plot, where the x-axis intercept of the curve (representing the energy in eV) was determined and recorded, as demonstrated in Figures (4.29 and 4.30).

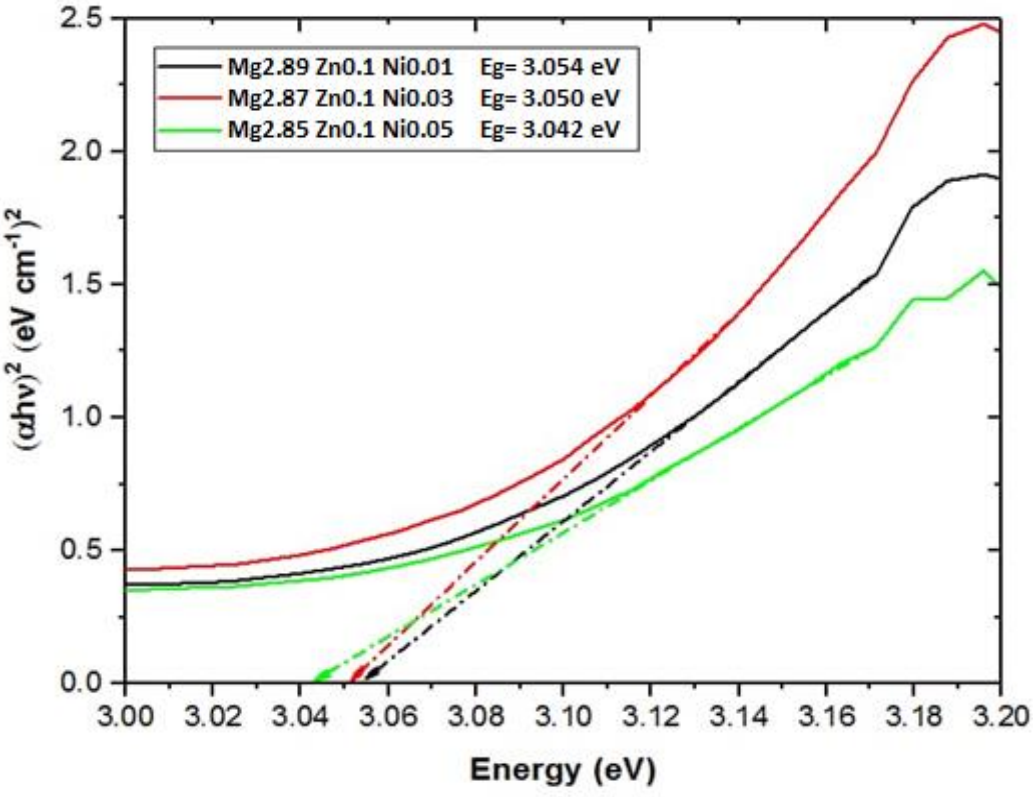

Figure 4.29. Tauc plot for MgZnNi/Al LDH band gap energy.

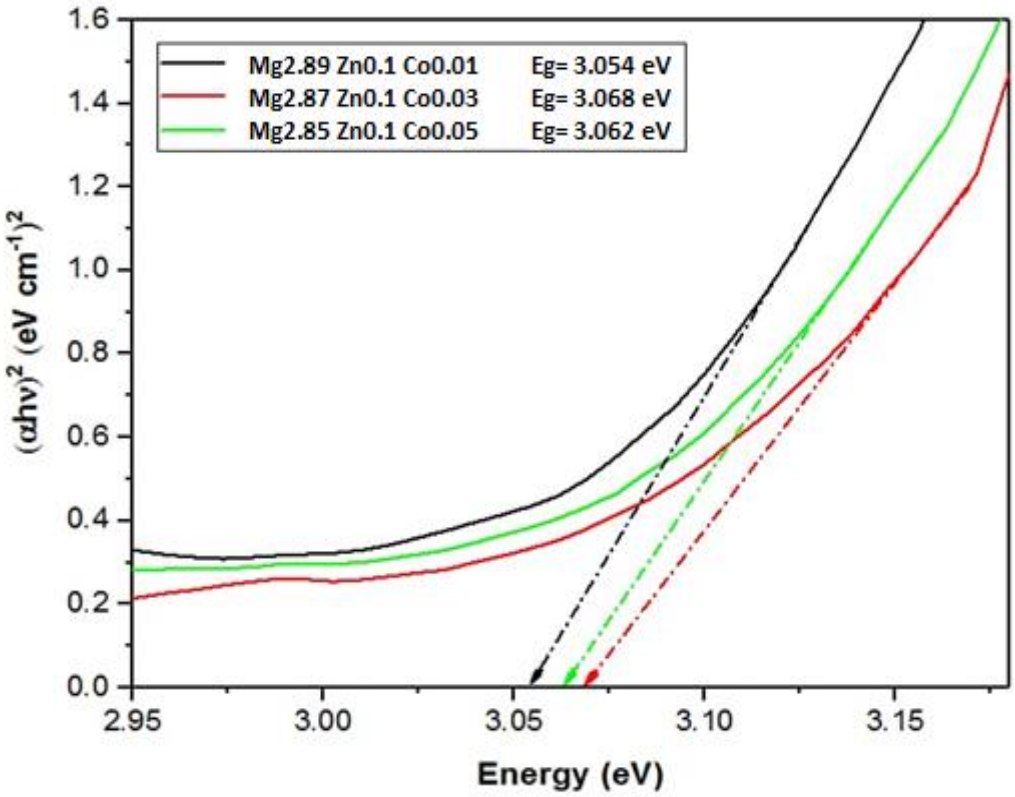

Figure 4.30. Tauc plot for MgZnCo/Al LDH band gap energy.

Based on the measurements obtained (given in Tabel 4.2), the band gap energy of $Mg_{3-x-y}Zn_xNi_y/Al_1$ LDH is in the range of 3.042–3.054 eV [72], exhibiting an inverse correlation with the nickel concentration as the band gap energy reasonably reduced when the amount of the nickel in the layered double hydroxide composition increased. Conversely, the optical band gap energy of $Mg_{3-x-y}Zn_xCo_y/Al_1$ LDH is in the range of 3.054-3.068 eV, the band gap energy increased to reach maximum value when the cobalt amount increased from y = 0.01 to y = 0.03 before experiencing a slight decrease at y = 0.05. Moreover, upon examining the acquired the optical band gap energy values for MgZnNi/Al LDH and MgZnCo/Al LDH, which exceed 3 eV, indicating the difficulty in exciting the s orbital electrons within the valence band, as a result, it can be inferred that these materials should be categorized as insulators and generally exhibit poor electrical conductivity. The optical band gap energy of MgZnM'/Al LDHs can be manipulated by structural alterations, which are influenced by the changes in morphology, particle size [73] and the incorporation of various metal cations [74], ultimately affecting the photocatalytic properties.

Furthermore, it's interesting to mention that the optical band energy of cobalt samples was consistently higher than the optical band gap energy of nickel samples with maximum band gap energy value (Eg = 3.054 eV) of nickel LDHs was equivalent to that of the minimum of cobalt LDHs. This observation indicates that the nickel LDHs appear to exhibit better electrical conductivity [75].

5. CONCLUSIONS

- The targeted compounds MgZnNi/Al LDH and MgZnCo/Al LDH nanoparticles were successfully fabricated via the sol-gel method, where the magnesium was partially replaced by two different metal cations (Zn^{2+} and Ni^{2+}) in the first LDH, likewise, (Zn^{2+} and Co^{2+}) in the second LDH.
- All three different desired concentrations of $Mg_{3-x-y}Zn_{\times}M_y/Al_1$ LDH (where, M = Ni or Co) nanoparticles were synthesized by varying the molar ratios of Mg to Ni and Mg to Co. Basically, the precursor metals cations solutions were prepared, followed by the controlled procedure of the sol-gel process to acquire LDH powders. Varying the molar ratio led to changes in the structural properties of LDH particles, moreover, influenced the depth of their colors.
- The synthesized LDH samples underwent characterization using various characterization techniques, including FT-IR spectroscopy, X-ray diffraction, and ultraviolet-visible spectroscopy. These techniques collectively offered a thorough understanding of the composition, structural and optical properties of the double metal substituted $Mg_{3-x-y}Zn_{\times}M_y/Al_1$ LDH.
- XRD data showed the presence of LDH structure and revealed similar patterns for the MgZnNi/Al LDH samples and MgZnCo/Al LDH samples, suggesting that they have a common structural backbone despite potential differences in their specific compositions.
- XRD data revealed that Nickel LDH samples have higher crystallinity than Cobalt LDH samples due to nickel's smaller atomic radius compared to cobalt's.
- The FT-IR data showed the distinct bands corresponding to the different vibrational modes of the functional groups within the LDH structure, notably (OH) and (NO_3) groups.
- The UV-Vis absorption and reflection spectra of MgZnNi/Al LDH exhibited peaks corresponding to pi-pi transitions of nickel and zinc metals. However, the nickel absorbance observed within the ultraviolet region suggests a high degree of structural arrangement.

- The XRD data were utilized to calculate the crystallite sizes' values, lattice constant, volume of unit cell, positions and displacements of the atoms, microstrain and the atomic packing factor (c/a).
- The computed values revealed that the average crystallite size of MgZnCo/Al LDH samples was larger than the crystallite size of MgZnNi/Al LDH samples, which equals to 9.86 nm and 9.14 nm, respectively. This confirmed that both materials fall within the nanoparticle range and indicating their effective formation at the nanoscale level.
- An inverse relationship was observed between the structural lattice parameters and the crystallite size. Furthermore, the atomic packing factor (c/a) was calculated using the values of the a and c parameters.
- The maximum unit cell volume for MgZnNi/Al LDH was observed at the third concentration, while it was at the second concentration for MgZnCo/Al LDH. This indicates that the chemical pressure should be at a minimum at these specific concentrations.
- Microstrain values for MgZnNi/Al LDH ranged from 16.5 to 19.2, while those for MgZnCo/Al LDH varied from 15.7 to 24.
- The UV-Vis data were utilized to calculate the band gap energies for both MgZnNi/Al LDH and MgZnCo/Al LDH which found to be exceeded 3 eV, indicating them as insulators with poor electrical conductivity.
- The band gap energy of MgZnNi/Al LDH ranges between 3.042–3.054 eV. It shows an inverse relationship with the nickel concentration, as the band gap energy decreases with the increase of nickel concentration.
- The $Mg_{3-x-y}Zn_xCo_y$/Al LDH optical band gap energy's values are higher than nickel containing LDH ranges from 3.054 to 3.068 eV, increasing as the cobalt concentration rises from y = 0.01 to y = 0.03, followed by a slight decrease at y = 0.05.
- The dielectric constant of $Mg_{3-x-y}Zn_xM'_y$/Al (M: Ni or Co) LDH exhibited a positive correlation with increasing nickel concentration, peaking at y=0.05, while decreasing with high cobalt concentrations, maximum at y = 0.01. Despite these variations, the dielectric constant values across all examined samples remained closely aligned, ranging from 7.89 to 7.94.

6. REFERENCES

Vancouver citation system was used in this thesis.

[1] M. Shahadat *et al.*, "A critical review on the prospect of polyaniline-grafted biodegradable nanocomposite," *Adv. Colloid Interface Sci.*, vol. 249, pp. 2–16, 2017.

[2] S. Tang and H. K. Lee, "Application of dissolvable layered double hydroxides as sorbent in dispersive solid-phase extraction and extraction by co-precipitation for the determination of aromatic acid anions," *Anal. Chem.*, vol. 85, no. 15, pp. 7426–7433, 2013.

[3] S. Tang, Y. Yao, T. Chen, D. Kong, W. Shen, and H. K. Lee, "Recent advances in the application of layered double hydroxides in analytical chemistry: A review," *Anal. Chim. Acta*, vol. 1103, pp. 32–48, 2020.

[4] E. Al-Khafaji, "Synthesis and Characterization of Ni/Al-LDH nano hybrid with (Ascorbic acid) and Kinetic Controlled Release Study of (Ascorbic acid) From Ni/Al-LDH," in *Journal of Physics: Conference Series*, IOP Publishing, 2020, p. 12026.

[5] M. Laipan *et al.*, "Functionalized layered double hydroxides for innovative applications," *Mater. Horizons*, vol. 7, no. 3, pp. 715–745, 2020.

[6] D. N. Ahmed, L. A. Naji, A. A. H. Faisal, N. Al-Ansari, and M. Naushad, "Waste foundry sand/MgFe-layered double hydroxides composite material for efficient removal of Congo red dye from aqueous solution," *Sci. Rep.*, vol. 10, no. 1, p. 2042, 2020.

[7] G. Mishra, B. Dash, and S. Pandey, "Layered double hydroxides: A brief review from fundamentals to application as evolving biomaterials," *Appl. Clay Sci.*, vol. 153, pp. 172–186, 2018.

[8] D. Tonelli, I. Gualandi, E. Musella, and E. Scavetta, "Synthesis and characterization of layered double hydroxides as materials for electrocatalytic applications," *Nanomaterials*, vol. 11, no. 3, p. 725, 2021.

[9] H. E. Salman and N. J. Hussein, "Synthesis of zinc-aluminum layered double hydroxides and application of adsorption for nitrate from water," in *IOP Conference Series: Materials Science and Engineering*, IOP Publishing, 2019, p. 12070.

[10] W. Zhou, Y. Li, S. Cheng, Y. He, J. Song, and Q. Zhang, "Synergistic Effects of Layered Double Hydroxide and MoS2 on the Performance of Lubricants," *Lubricants*, vol. 12, no. 5, p. 155, 2024.

[11] D. Tonelli, E. Scavetta, and M. Giorgetti, "Layered-double-hydroxide-modified electrodes: electroanalytical applications," *Anal. Bioanal. Chem.*, vol. 405, pp. 603–614, 2013.

[12] B. Habibi, A. Pashazadeh, S. Pashazadeh, and L. A. Saghatforoush, "A new method for the preparation of MgAl layered double hydroxide-copper metal–organic frameworks structures: application to electrocatalytic oxidation of formaldehyde," *Sci. Rep.*, vol. 14, no. 1, pp. 1–17, 2024.

[13] Y. Zhao *et al.*, "Layered-double-hydroxide nanosheets as efficient visible-light-driven photocatalysts for dinitrogen fixation," *Adv. Mater.*, vol. 29, no. 42, p. 1703828, 2017.

[14] Y. Zhao *et al.*, "Alkali etching of layered double hydroxide nanosheets for enhanced photocatalytic N2 reduction to NH3," *Adv. energy Mater.*, vol. 10, no. 34, p. 2002199, 2020.

[15] A. Razzaq, S. Ali, M. Asif, and S.-I. In, "Layered double hydroxide (LDH) based photocatalysts: An outstanding strategy for efficient photocatalytic CO2 conversion," *Catalysts*, vol. 10, no. 10, p. 1185, 2020.

[16] R. Benhiti *et al.*, "Synthesis, characterization, and comparative study of MgAl-LDHs

prepared by standard coprecipitation and urea hydrolysis methods for phosphate removal," *Environ. Sci. Pollut. Res.*, vol. 27, pp. 45767–45774, 2020.

[17] C. Jaramillo-Hernández, V. Oestreicher, M. Mizrahi, and G. Abellán, "Upscaling the urea method synthesis of CoAl layered double hydroxides," *Beilstein J. Nanotechnol.*, vol. 14, no. 1, pp. 927–938, 2023.

[18] J. Prince, A. Montoya, G. Ferrat, and J. S. Valente, "Proposed general sol− gel method to prepare multimetallic layered double hydroxides: synthesis, characterization, and envisaged application," *Chem. Mater.*, vol. 21, no. 24, pp. 5826–5835, 2009.

[19] H. Griffiths, "Layered double hydroxides: structure, synthesis and catalytic applications." University of Huddersfield, 2012.

[20] Z. M. Mir, A. Bastos, D. Höche, and M. L. Zheludkevich, "Recent advances on the application of layered double hydroxides in concrete—A review," *Materials (Basel).*, vol. 13, no. 6, p. 1426, 2020.

[21] M. R. Berber, I. H. Hafez, K. Minagawa, M. Katoh, T. Mori, and M. Tanaka, "Uniform nanoparticles of hydrotalcite-like materials and their textural properties at optimized conditions of urea hydrothermal treatment," *J. Mol. Struct.*, vol. 1033, pp. 104–112, 2013.

[22] S. Park, D. Kwon, J. Y. Kang, and J. C. Jung, "Influence of the preparation method on the catalytic activity of MgAl hydrotalcites as solid base catalysts," *Green Energy Environ.*, vol. 4, no. 3, pp. 287–292, 2019.

[23] X. Liu, Y. Shao, Y. Zhang, G. Meng, T. Zhang, and F. Wang, "Using high-temperature mechanochemistry treatment to modify iron oxide and improve the corrosion performance of epoxy coating–I. High-temperature ball milling treatment," *Corros. Sci.*, vol. 90, pp. 451–462, 2015.

[24] Q. Wang and D. O'Hare, "Recent advances in the synthesis and application of layered double hydroxide (LDH) nanosheets," *Chem. Rev.*, vol. 112, no. 7, pp. 4124–4155, 2012.

[25] E. Rahmani, "Preparation and Characterization of Thin Films by Sol-Gel Method," in *Thin Films-Growth, Characterization and Electrochemical Applications*, IntechOpen, 2023.

[26] G. Lee, J. Y. Kang, N. Yan, Y.-W. Suh, and J. C. Jung, "Simple preparation method for Mg–Al hydrotalcites as base catalysts," *J. Mol. Catal. A Chem.*, vol. 423, pp. 347–355, 2016.

[27] A. Hassen, A. M. El Sayed, A. Al-Ghamdi, and M. Shaban, "Synthesis of Some Functional Oxides and Their Composites Using Sol-Gel Method," in *Sol-Gel Method-Recent Advances*, IntechOpen, 2023.

[28] R. Wahab, S. G. Ansari, M. A. Dar, Y. S. Kim, and H. S. Shin, "Synthesis of magnesium oxide nanoparticles by sol-gel process," in *Materials Science Forum*, Trans Tech Publ, 2007, pp. 983–986.

[29] S. M. Simon *et al.*, "Recent advancements in multifunctional applications of sol-gel derived polymer incorporated TiO_2-ZrO_2 composite coatings: A comprehensive review," *Appl. Surf. Sci. Adv.*, vol. 6, p. 100173, 2021.

[30] A. V. Rao, S. D. Bhagat, H. Hirashima, and G. M. Pajonk, "Synthesis of flexible silica aerogels using methyltrimethoxysilane (MTMS) precursor," *J. Colloid Interface Sci.*, vol. 300, no. 1, pp. 279–285, 2006.

[31] J. Qu, L. Sha, C. Wu, and Q. Zhang, "Applications of mechanochemically prepared layered double hydroxides as adsorbents and catalysts: A mini-review," *Nanomaterials*, vol. 9, no. 1, p. 80, 2019.

[32] J. Zhang, Y. F. Xu, G. Qian, Z. P. Xu, C. Chen, and Q. Liu, "Reinvestigation of dehydration and dehydroxylation of hydrotalcite-like compounds through combined TG-DTA-MS

analyses," *J. Phys. Chem. C*, vol. 114, no. 24, pp. 10768–10774, 2010.

[33] Molano-Mendoza M. , Donneys-Victoria D. , Marriaga-Cabrales N. , Mueses M. , Puma G. , & Machuca-Martínez F.. Synthesis of mg-al layered double hydroxides by electrocoagulation. MethodsX 2018; 5:915-923.

[34] Chen Y., Li F., Zhou S., Wei J., Dai Y., & Chen Y. The fluorescence of Mg–Al–Eu ternary layered hydroxides response to tryptophan. Luminescence 2011;27(3):223-228.

[35] Udourioh, G., Solomon, M., Matthews-Amune, C., Epelle, E., Agbazue, V., & Onyenze, U. (2023). current trends in the synthesis, characterization and application of metal-organic frameworks. reaction chemistry & engineering, 8(2), 278-310

[36] Shi, W., Lin, Y., Zhang, S., Tian, R., Liang, R., Wei, M., … & Duan, X. (2013). study on Uv-shielding mechanism of layered double hydroxide materials. physical chemistry chemical physics, 15(41), 18217.

[37] Smalenskaite A. , Vieira D. , Salak A. , Ferreira M. , Katelnikovas A. , & Kareiva A.. A comparative study of co-precipitation and sol-gel synthetic approaches to fabricate cerium-substituted mg al layered double hydroxides with luminescence properties. Applied Clay Science 2017; 143:175-183.

[38] Carlino S., Hudson M., Husain S., & Knowles J. The reaction of molten phenylphosphonic acid with a layered double hydroxide and its calcined oxide. Solid State Ionics 1996;84(1-2):117-129.

[39] Carlino S, Hudson MJ. Reaction of molten sebacic acid with a layered (Mg/Al) double hydroxide. J Mater Chem. 1994;4(1):99–104.

[40] Khan, Y., et al. "Optical properties of layered double hydroxides: A review." *Journal of Materials Chemistry C* 2020, 8(12), 4050-4065.

[41] Li, Y., et al. "Layered double hydroxides: Synthesis, properties, and applications." *Journal of Solid State Chemistry* 2018, 261, 1-12.

[42] Zhang, Y., et al. "Tuning the electronic properties of layered double hydroxides by metal cation substitution." *Applied Clay Science* 2019, 182, 105-112.

[43] Zhou, Y., et al. "Magnetic properties of layered double hydroxides: A review." *Journal of Magnetism and Magnetic Materials* 2021, 526, 167-178.

[44] Marzec A. , Szadkowski B. , Rogowski J. , Maniukiewicz W. , Rybiński P. , & Prochoń M.. New organic/inorganic pigments based on azo dye and aluminum-magnesium hydroxycarbonates with various mg/al ratios. Materials 2019;12(8):1349.

[45] Chen, Y., et al. "Defects in layered double hydroxides: Implications for color and electronic properties." *Applied Clay Science* 2020, 185, 105408.

[46] Zhao, Y., et al. "Synthesis and characterization of layered double hydroxides with tunable morphology." *Journal of Solid State Chemistry* 2020, 284, 121-130.

[47] Smalenskaite A. , Vieira D. , Salak A. , Ferreira M. , Katelnikovas A. , & Kareiva A.. A comparative study of co-precipitation and sol-gel synthetic approaches to fabricate cerium-substituted mg al layered double hydroxides with luminescence properties. Applied Clay Science 2017; 143:175-183.

[48] Wang, Z., et al. "Thermal Dehydration of Layered Double Hydroxides: A Review." *Applied Clay Science* 2014, 87, 1-10

[49] Zeng, H., et al. "Thermal Stability and Dehydration of Layered Double Hydroxides." *Journal of Solid State Chemistry* 2015, 229, 1-8.

[50] Pitchi C., Priyadarshini A., & Narala S. Synthesis of tio2 coatings by thermal oxidation with

a suitable cooling process for improved wettability. Surface Engineering 2021;37(12):1586-1595.

[51] Zhang F., Chupas P., Lui S., Hanson J., Caliebe W., Lee P. et al. In situ study of the crystallization from amorphous to cubic zirconium oxide: rietveld and reverse monte carlo analyses. Chemistry of Materials 2007;19(13):3118-3126.

[52] Wang H, Chen Y, Xie W, Han X, Feng Q, Jiang R, et al. Construction of highly active Pt/Ni-Fe layered double hydroxide electrocatalyst towards methanol oxidation in alkaline medium. International Journal of Electrochemical Science 2019;14(8):7961-7972.

[53] Gamil S., Rouby W., Antuch M., & Zedan I. Nanohybrid layered double hydroxide materials as efficient catalysts for methanol electrooxidation. RSC Advances 2019;9(24):13503-13514.

[54] Ma K., Cheng J., Liu F., & Zhang X. Co-Fe layered double hydroxides nanosheets vertically grown on carbon fiber cloth for electrochemical capacitors. Journal of Alloys and Compounds 2016; 679:277-284.

[55] Badreddine M., Khaldi M., Legrouri A., Barroug A., Chaouch M., Roy A. et al. Chloride-hydrogenophosphate ion exchange into the zinc–aluminium–chloride layered double hydroxide. Materials Chemistry and Physics 1998;52(3):235-239.

[56] Shabanian M., Hajibeygi M., & Raeisi A. FTIR characterization of layered double hydroxides and modified layered double hydroxides. Layered Double Hydroxide Polymer Nanocomposites 2020:77-101.

[57] Hajibeygi M., Shabanian M., & Omidi-Ghallemohamadi M. Development of new acid-imide modified Mg-Al/LDH reinforced semi-crystalline poly(amide-imide) containing naphthalene ring; study on thermal stability and optical properties. Applied Clay Science 2017; 139:9-19.

[58] Singh J. and Bahel S. Rietveld refinements, crystal structure and uv–vis spectroscopy of MgO and $Mg(OH)_2$-based undoped and Sn^{4+}-doped $MgTiO_3$ ceramics. Materials Today: Proceedings 2021; 45:5249-5254.

[59] Aksay S. Effects of al dopant on XRD, FT-IR and Uv–vis properties of MgO films. Physica B: Condensed Matter 2019; 570:280-284.

[60] Gevers B., Naseem S., Sheppard C., Leuteritz A., & Labuschagne F. Modification of layered double hydroxides using first-row transition metals for superior Uv-Vis-NIR absorption and the influence of the synthesis method used. 2020.

[61] Zakaria S. , Amini M. , & Ahmadi S.. Noninvasive colorimetric detection of acetic acid in human breath based on an alginate/Ni–Al-LDH/dye composite film. ACS Omega 2023;8(26):23613-23621.

[62] Kovalenko V. and Kotok V.. Improvement of continuous technology of electrochemical synthesis of nickel hydroxide by implementation of solution recycling. Eastern-European Journal of Enterprise Technologies 2021;1(6 (109)):30-38.

[63] Scherrer P.. Bestimmung der inneren struktur und der größe von kolloidteilchen mittels röntgenstrahlen. Kolloidchemie Ein Lehrbuch 1912:387-409.

[64] Mustapha S., Ndamitso M., Abdulkareem A., Tijani J., Shuaib D., Mohammed A. et al. Comparative study of crystallite size using williamson-hall and debye-scherrer plots for ZnO nanoparticles. Advances in Natural Sciences: Nanoscience and Nanotechnology 2019;10(4):045013.

[65] Ismail, M. A., Taha, K. K., Modwi, A., & Khezami, L. ZnO nanoparticles: Surface and X-ray profile analysis. *J. Ovonic Res*, 2018, 14.5: 381-393.

[66] Nandiyanto A., Triawan F., Firly R., & Kishimoto K. Crystallite size on micromechanical characteristics of wo3 microparticles. Journal of Engineering Research 2021;9(3A).

[67] Zhao Z. and Du L. Quantitative relationship between crystallite size and adhesion strength of the electroforming layer during microelectroforming process. Micro &Amp; Nano Letters 2015;10(2):64-66.

[68] Şenol S., Yalçın B., Özuğurlu E., & Arda L. Structure, microstructure, optical and photocatalytic properties of Mn-doped ZnO nanoparticles. Materials Research Express 2020;7(1):015079.

[69] Şenol S., Özuğurlu E., & Arda L. Synthesis, structure and optical properties of (Mn/Cu) Co-doped ZnO nanoparticles. Journal of Alloys and Compounds 2020; 822:153514.

[70] Rahimi F., Rahmati A., & Mardani S. Determination and analysis of structural and optical properties for thermally evaporated ZnO thin films. Soft Nanoscience Letters 2014;04(01):1-5.

[71] M. Tosun, S.D. Senol, L. Arda, Effect of Mn/Cu co-doping on the structural, optical and photocatalytic properties of ZnO nanorods. Journal of Molecular Structure, Volume 1212,2020,128071, ISSN 0022-2860.

[72] Xu S., Pan T., Dou Y., Yan H., Zhang S., Ning F. et al. Theoretical and experimental study on $M^{ii}M^{iii}$-layered double hydroxides as efficient photocatalysts toward oxygen evolution from water. The Journal of Physical Chemistry C 2015;119(33):18823-18834.

[73] Tan L. , Xu S. , Wang Z. , Xu Y. , Wang X. , Hao X. et al.. Highly selective photoreduction of CO_2 with suppressing H_2 evolution over monolayer layered double hydroxide under irradiation above 600 nm. Angewandte Chemie International Edition 2019;58(34):11860-11867.

[74] Sherryna A. and Tahir M. Recent developments in layered double hydroxide structures with their role in promoting photocatalytic hydrogen production: a comprehensive review. International Journal of Energy Research 2021;46(3):2093-2140.

[75] Yan H. , Wei M. , Ma J. , Evans D. , & Duan X. Plane-wave density functional theory study on the structural and energetic properties of cation-disordered Mg−Al layered double hydroxides. The Journal of Physical Chemistry A 2010;114(27):7369-7376.